The Strong Isospin-Breaking Correction to the Leading-Order Hadronic Vacuum Polarisation Contribution to the Anomalous Magnetic Moment of the Muon

Christopher Lewis James

A Thesis Submitted to
the Faculty of Graduate Studies
in Partial Fulfillment of the Requirements
for the degree of Master of Science

Graduate Program in Physics and Astronomy
York University
Toronto, Ontario

Abstract

The contribution of strong isospin-breaking (SIB) effects to the value of the anomalous magnetic moment of the muon is studied using the leading-order SIB component of the photon vacuum polarisation function, calculated in Chiral Perturbation Theory (ChPT) in the low Euclidean momentum-squared regime. At two-loop order in ChPT the result is found to be $a_\mu^{SIB} = 0.82(12) \times 10^{-10}$, approximately 1 order of magnitude less than recent determinations using Lattice Quantum Chromodynamics (QCD) and also phenomenology. It is shown that the inclusion of a tree-level term from next-to-next-to-next-to leading order (NNNLO) raises the ChPT prediction to $a_\mu^{SIB} = 3.61(98) \times 10^{-10}$. This result is consistent with the most precise result from Lattice QCD. The dominant NNNLO contribution is interpreted as parameterising the SIB physics of the lightest resonances which are predicted to be the most significant processes at low momentum.

Acknowledgements

I would like to thank my supervisors Kim Maltman and Randy Lewis for their generous guidance and support throughout the last two years. The insights I have gained from our discussions have been invaluable and without them this thesis would not be possible.

Table of Contents

List of Tables

List of Figures

Chapter 1

Introduction

1.1 The Anomalous Magnetic Moment of the Muon Problem

The anomalous magnetic moment of the muon is the subject of substantial interest in the high-energy physics community. The evidence of an at-present statistically significant difference between the experimental and theoretical results for this property provides motivation for the ongoing escalation of efforts on both sides to reach a definitive conclusion as to whether this discrepancy is real, or represents a statistical fluctuation. Furthermore, the relevance of the anomaly to the search for Beyond-the-Standard-Model (BSM) physics has been amplified by a lack of evidence from energy-frontier experiments carried out using the Large Hadron Collider (LHC) at CERN [13]. Rather than as a secondary search method, the muon anomaly is elevated in status by the precision at which it can be measured experimentally. This experimental precision offers theorists an opportunity to test the Standard Model at remarkably small scales and place new limits on the nature of any possible deviations that would signal the breakdown of our current understanding of elementary particle physics.

The anomalous magnetic moment of the muon is a feature of the interaction between the muon and the electromagnetic field. One can imagine, instead of a point particle, a

planar current loop placed into a magnetic field, as in Fig. 1.1. The magnetic moment of the loop will prefer to align itself with the direction of the field in order to minimise energy. However the angular momentum of the current will instead cause the loop to enter a precession about the axis of the magnetic field, like a spinning top changing the orientation of its rotational axis. This simplification acts as a starting point for understanding how a point particle with a given spin interacts with the electromagnetic field. The gyromagnetic ratio, g, parameterising this behaviour is an observable predicted in a relativistic quantum mechanics formulation to equal 2 by Dirac in 1928 [14]. The anomalous magnetic moment, $a_\ell \equiv (g_\ell - 2)/2$, is measured as the deviation from Dirac's prediction, hence the problem is commonly referred to as "$g-2$". This nomenclature will be used frequently throughout this thesis.

All leptons, the electron, muon and tau, and their respective antiparticles are point particles, as opposed to a proton, for example, which is a composite particle made up of quarks and gluons. They are spin-1/2 fermions with electric charge $-e$ for the standard leptons and $+e$ for their antiparticle partners, where, by convention, e is chosen to be positive. Setting aside the antiparticles, the three lepton generations possess all the same properties except for mass. The electron mass is $m_e = 0.511$ MeV [1], the muon is approximately 200 times heavier at $m_\mu = 105.658$ MeV [1], and the tau is approximately 3500 times heavier than the electron at $m_\tau = 1776.86$ MeV [1]. Their masses and corresponding lifetimes make each lepton a unique experimental prospect in the context of $g-2$ physics. The electron is by far the best understood in the sense of the agreement between experimental [1] and theoretical results [15],

$$a_e^{exp} = 1159652180.91(26) \times 10^{-12},$$
$$a_e^{SM} = 1159652181.606(11)(12)(229) \times 10^{-12}.$$

Clearly the Standard Model provides an excellent description of the electron's magnetic moment. Yet as Jegerlehner states in his book *The Anomalous Magnetic Moment of the*

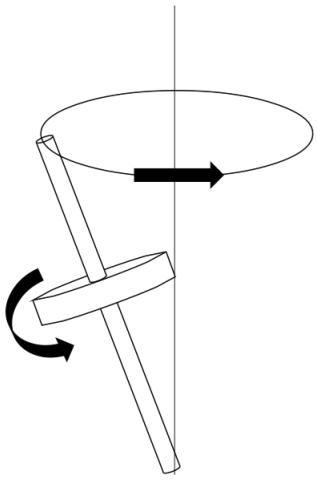

Figure 1.1: Precession of a spinning top analogous to the spin precession of the muon inside a homogeneous magnetic field.

Muon [3],

"As a matter of principle, an experimentally determined quantity always includes all effects, known and unknown, existing in the real world. This includes electromagnetic, strong, weak and gravitational interactions, plus whatever effects we might discover in the future."

The as-of-yet undiscovered effects referred to in this quotation are an acknowledgement of the shortcomings of the Standard Model. Dark matter, dark energy, matter-antimatter asymmetry, neutrino oscillations, the strong CP problem, and quantum gravity are all topics in high-energy physics which are not explained by the Standard Model, but for which new exotic particles may provide solutions. A lepton's anomalous magnetic moment provides a probe for studying the contribution of any potential BSM physics and its sensitivity to these effects scales with the mass-squared of the lepton, m_ℓ^2 [3]. Therefore the muon BSM sensitivity is increased by a factor of approximately 40,000 compared with the electron. This scaling up of sensitivity suggests that the tau represents the best prospect of seeing new physics by a further factor of approximately 280 from the muon and therefore is the most interesting to study from a BSM point of view among the three

lepton anomalous magnetic moments. However, the short tau proper lifetime, $\mathcal{O}(10^{-13}\,\mathrm{s})$, prevents the application of the spin precession methods used to study a_e and a_μ and makes a_τ experimentally inaccessible at the level of precision achieved for the electron and muon. Measurements have been made, the most precise of which was from DELPHI, one of the detectors at the Large Electron Positron Collider [1,16], but this determination is an order of magnitude less precise than needed to begin to test the Standard Model prediction [17]:

$$a_\tau^{exp} = 0.018(17)$$
$$a_\tau^{SM} = 0.00117721(5).$$

A new proposal for studying a_τ from LHC heavy ion collisions has been made [18] aiming at opening up a_τ as a new precision pathway in the search for BSM physics.

Interest in the anomalous magnetic moment of the muon is currently particularly high because the existing tantalysing discrepancy with the Standard Model prediction will soon be tested to higher accuracy, with a new dedicated experiment currently running at Fermilab (the E989 experiment) [19–21], and the E34 experiment at J-PARC in Japan [22,23] expected to begin running in the near future. The predecessor of the Fermilab experiment was the long running E821 experiment at Brookhaven National Laboratory (BNL) [24]. The BNL experiment achieved a precision of 0.54 ppm and alongside theoretical efforts established the current 3-4 σ difference between experiment [1] and the SM prediction [1] (see also Refs. [25,26]),

$$a_\mu^{exp} = 11659209.1(5.4)(3.3) \times 10^{-10}$$
$$a_\mu^{SM} = 11659182.3(0.1)(3.4)(2.6) \times 10^{-10}$$

Before its move to BNL, the first measurements of a_μ were made at CERN in a series of three experiments [27–29] which first reached the level of precision at which it was important to include the $\sim$60 ppm contribution to a_μ from the hadronic vacuum polarisation.

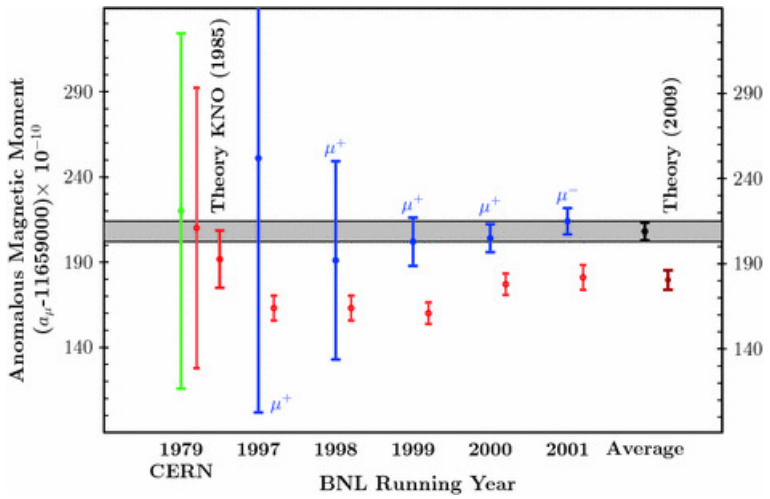

Figure 1.2: Results of the E821 experiments since 1979. The green result is the final CERN measurement and the blue bars are results from the BNL experiment. Shown here also are the theoretical predictions (red vertical bars) and new world average (gray bar) [3]. Data taken using nearly equal samples of both μ^- and μ^+ have been used to calculate a_μ, assuming the effect is the same for both matter and antimatter. The experimental error bars here show the combined statistical and systematic errors. The theoretical error bars are the combined uncertainties from the various SM sector contributions. Source: Jegerlehner, 2017 [3].

The results from 1979 onwards, marking the relocation of the experimental program to BNL, are shown in Fig. 1.2.

The method employed by the E989 experiment at Fermilab is the same as the one used at BNL. The current experiment even inherited the storage ring from BNL which made a 500 km journey across land and water to its present location. Muons, generated from pion decays, enter a homogeneous magnetic field where they undergo Larmor spin precession with a constant frequency. The spin precession is tracked through the decay of a muon to an electron, electron neutrino and muon neutrino,

$$\mu^- \to e^- + \bar{\nu}_e + \nu_\mu \quad , \quad \mu^+ \to e^+ + \nu_e + \bar{\nu}_\mu$$

where the electrons are emitted preferentially with momentum in the opposite direction to the muon spin polarisation. The anomalous precession angular frequency, ω, in a homoge-

neous magnetic field, $\vec{B}$, is related to a_μ via

$$\vec{\omega} = -\frac{e}{m_\mu}\left[a_\mu \vec{B} - \left(a_\mu - \frac{1}{\gamma^2 - 1}\right)\vec{\beta} \times \vec{E}\right]. \tag{1.1}$$

where m_μ is the muon mass, e is the electron charge, γ is the Lorentz factor, $\vec{\beta}$ is the velocity, and $\vec{E}$ is the electric field used to constrain the muon beam in the detector [30]. By keeping the muons at the so called 'magic' momentum of approximately 3.1 GeV, the coefficient of the cross product term vanishes and the expression reduces to

$$\vec{\omega} = -\frac{e}{m_\mu} a_\mu \vec{B}. \tag{1.2}$$

The observables actually measured in the Fermilab experiment are ω, the electron g factor, the electron mass, m_e, the electron magnetic moment, μ_e, the muon-distribution-weighted average proton Larmor precession frequency in the storage ring's field, $\tilde{\omega}_p$, and the proton magnetic moment, μ_p. The experimental value of a_μ is then determined from those observables via [31],

$$a_\mu = \frac{g_e}{2}\frac{\omega}{\tilde{\omega}_p}\frac{m_\mu}{m_e}\frac{\mu_p}{\mu_e}. \tag{1.3}$$

The target total uncertainty of the Fermilab experiment, split evenly between systematics and statistics, is 140 ppb [20] to be achieved through a combination of improved systematics and 20 times the number of muons available in the BNL analysis. The experiment completed its first run during the Spring of 2018 with six independent teams showing excellent agreement in their determinations of the anomalous precession frequency, ω. The results for a_μ are expected to be released sometime in early 2020. Run 2 of the experiment began in Spring 2019, and Run 3 is scheduled to occur during 2019-2020. Were the central value of the new experimental result to turn out the same as the BNL result, the improved error of the Fermilab experiment would establish the discrepancy between experiment and the Standard Model prediction at the $>5\sigma$ level, the standard threshold for discovery in the field.

The alternative experiment seeking to measure a_μ is J-PARC E34 in Japan. This involves a novel approach working with ultra cold muons. In the experiment, slow polarized muons are injected at zero transverse momentum into a compact cylindrical trap filled with a homogeneous magnetic field. At these low energies, the experiment avoids the use of electric fields to control the muon beam and hence the precession frequency once again reduces to Eq. 1.2.

The slow-moving muons in the J-PARC experiment have lab-frame lifetimes much shorter (by a factor of $\sim$10) than those in the Fermilab experiment but move inside far smaller trapping devices of almost table top size. This smaller size means the experiment can use smaller magnetic fields which are intrinsically more uniform. The value of a_μ is once again measured by detecting the spin precession through the related modulation of the direction of the decay electrons and positrons. This experiment will provide an important cross check on the results which emerge from Fermilab.

The high interest in the muon anomalous magnetic moment discrepancy should not cause us to lose sight of the fact that the Standard Model successfully describes the vast majority of the experimentally observed lepton anomalous magnetic moments. The electron anomalous moment is one the most precisely measured quantities in all of physics and the SM provides a tremendously successful prediction of it. Both the muon and electron measurements are sensitive to all sectors of the SM allowing for precision tests of the individual electromagnetic, weak and strong sectors at new scales. The contribution from quantum electrodynamics (QED), responsible for 99% of the anomalous behaviour of the electron and muon has been calculated using perturbation theory to 5-loop order (10^{th} order in the QED coupling) [32, 33]. The summation of the different sector contributions gives the full SM prediction,

$$a_\mu^{SM} = a_\mu^{QED} + a_\mu^{EW} + a_\mu^{QCD} \tag{1.4}$$

where EW and QCD stand for electroweak and quantum chromodynamics (the theory of

the strong force) respectively.

The EW contribution results from effects involving the virtual exchange of the heavy weak gauge bosons $W^{\pm}$ and the Z, mediators of charged current and neutral current interactions respectively. The total EW contribution to a_μ is [1]

$$a_\mu^{EW} = 153.6(1.0) \times 10^{-11} \tag{1.5}$$

while the QED contribution is [1]

$$a_\mu^{QED} = 116584718.95(8) \times 10^{-11}. \tag{1.6}$$

Some of the more technical details of the QED and EW contributions are elucidated briefly in the Theoretical Background section.

The largest uncertainty in the SM prediction comes from the QCD contribution, specifically from uncertainties in the leading-order hadronic vacuum polarisation (LO-HVP) and hadronic light-by-light (HLbL) contributions [34]. A first principles determination of these contributions is made difficult by the properties of the QCD coupling constant which grows large at small energies preventing the use of traditional perturbation theory techniques in that energy region.

Currently the HVP contribution is evaluated from dispersion relations using experimental cross-section data of the electron-positron annihilation to hadrons ($e^+e^- \to$ hadrons) process. The HLbL contribution (see Refs. [35–37]) has been calculated using various models which cause the theoretical result to suffer from uncontrollable uncertainties. The identification of the hadronic contributions as the source of the largest theoretical uncertainties in the SM prediction of a_μ has fuelled several research efforts into both the HVP and the HLbL determinations. One approach that has had notable success is Lattice QCD (LQCD), a method based upon the discretisation of spacetime allowing, in principle, the calculation of QCD effects from first principles. RBC-UKQCD, BMW, Mainz, Fermilab-

HPQCD-MILC, and ETM are all collaborations studying the hadronic contribution to a_μ through LQCD that have published results for the leading-order part of the HVP in recent years. A review of results prior to 2019 is available in Ref. [26].

The evaluation of the hadronic part of a_μ from first principles involves handling hadronic contributions at both low and high energies and therefore LQCD is favourable since its formulation offers a way of performing low energy QCD calculations. LQCD results are determined from resource-intensive numerical simulations requiring access to supercomputers. It is important for the results of these simulations to be checked against other methods. At high energies these checks can be provided by QCD perturbation theory, since the coupling grows small as energy becomes large. At low energies effective field theories can also provide useful analytical constraints for LQCD studies.

The main subject of this thesis is the use of chiral perturbation theory, an effective field theory of QCD at low energies, to provide a constraint on LQCD results for the contribution of strong isospin breaking (SIB) to the LO-HVP. SIB processes are those which arise from the small mass difference between the up and down quarks in QCD. The target improved precision of the current generation of muon $g-2$ experiments will no longer allow the very small SIB corrections to be neglected in LQCD determinations, especially of the LO-HVP contribution. An estimate of the scale of SIB effects from scale of the $u-d$ quark mass difference compared with the QCD scale, Λ_{QCD},

$$\frac{m_d - m_u}{\Lambda_{QCD}} \sim 1\% \tag{1.7}$$

predicts the appearance of SIB physics at $\mathcal{O}(10^{-10})$ based on the size of the current theoretically determined HVP contribution to a_μ [1],

$$a_\mu^{LO-HVP} = 6931(33)(7) \times 10^{-11} \tag{1.8}$$

which dominates in numerical size over the HLbL contribution. Current LQCD studies aim

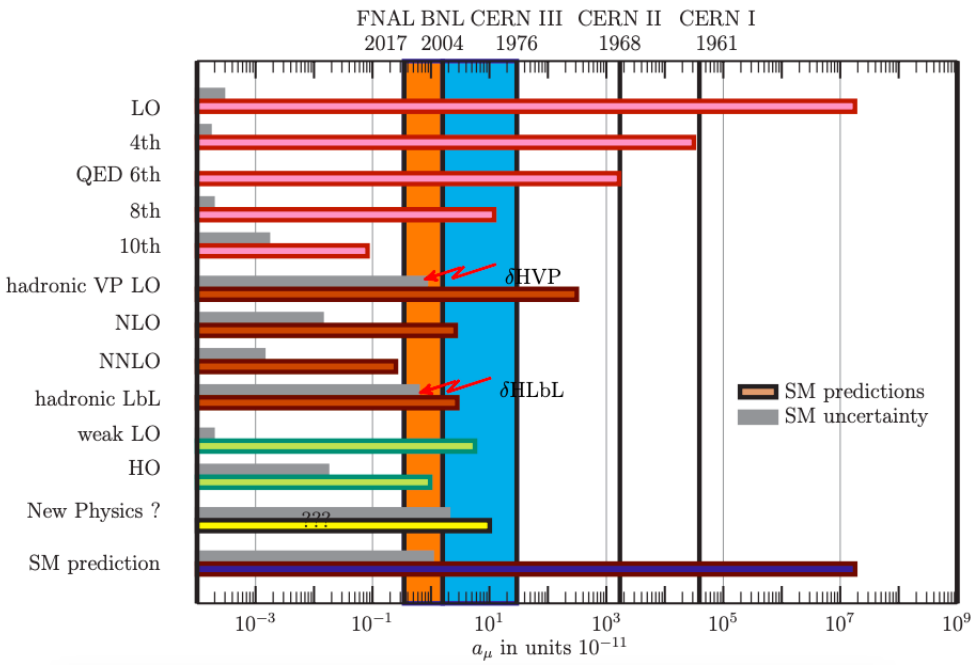

Figure 1.3: The contributions of the various sectors of the SM to the value of a_μ (coloured horizontal lines) and their associated uncertainties (gray horizontal lines) displayed against the precision reached by $g-2$ experiments (vertical bands). The blue band here shows the increase in precision over the course of the BNL experiment (1976 to 2004). The orange band shows the increased precision targeted by the Fermilab experiment. The 'New Physics?' included in this figure shows the value $(a_\mu^{exp} - a_\mu^{SM})/a_\mu^{exp})$. Source: Jegerlehner, 2017 [3].

to eventually resolve the HVP to a precision of $\mathcal{O}(0.1\%)$ [26] ($\mathcal{O}(10^{-11})$). SIB corrections are therefore an essential part of the QCD piece of the SM prediction for a_μ. A comparison of the sizes of the various determinations of SM sector contributions and their uncertainties is shown in comparison with the scales of the BNL experimental results and the target scales of the new generation experiments in Figure 1.3.

Although the focus of this thesis is on improving the precision of the SM prediction for a_μ, one should bear in mind that the interest in doing so is connected with the possibility that new physics will expose itself in the new muon $g-2$ measurement results. This possibility acts as the major driving force in the world-wide effort to study this problem. The fact that so far in LHC experiments at the high-energy frontier no results have arisen which cannot be explained by the SM is cause for a great deal of consternation in the HEP community. In a 2018 blog article for Scientific American, neutrino physicist Jonathan Link

summed up the sentiment of those frustrated by the current state of affairs by describing the SM as a 'tyrant' whose 'apparent infallibility saps the vitality of the field'. Were the new $g-2$ experiments to produce results in agreement with the SM prediction, this would likely compound these problems and force hopes to turn once more to the energy frontier, to future runs of the upgraded LHC experiments [38] and, beyond that, to the possibility of the proposed Future Circular Collider (FCC) [39]. There remains, however, the possibility that the new Fermilab result could establish the muon $g-2$ discrepancy at the >4-5σ level, a result which, in the field, would be considered to represent the unambiguous discovery of BSM physics contributions.

A vast landscape of BSM theories exist. Fourth generation *sequential* fermions with a heavy neutrino, extensions to the Higgs sector, supersymmetry, and dark matter are just a few of the great many speculations on new physics. The results of the $g-2$ experiment may be used to place constraints on new physics. Berestetskii et al. [40, 41] found in 1956 that the QED momentum cutoff for four-momentum transfer at $q^2 = \Lambda^2$ meant that the sensitivity of a_ℓ to new physics scaled as

$$\frac{\delta a_\ell}{a_\ell} \sim \frac{m_\ell^2}{\Lambda^2} \tag{1.9}$$

where δa_ℓ here would represent the discrepancy between SM theory and experiment were this discrepancy to be the result of BSM contributions. This reinforces the earlier statement that the muon is a far better probe of the short distance region where new physics is expected to become accessible. The cutoff Λ sets the scale of the new physics, which if one assumes such new physics to have the form of previously unseen states of mass M_{NP} leads us to a general expression for the BSM contribution to a_μ,

$$a_\mu^{NP} = \mathcal{C}\frac{m_\mu^2}{M_{NP}^2} \tag{1.10}$$

where $\mathcal{C} = \mathcal{O}(\alpha/\pi)$ [3]. If one takes the difference between the current central values of the

results from experiment and theory, the size of the discrepancy is $\sim 27 \times 10^{-10}$. (The paper by Blum et al. [25] lists multiple values of the discrepancy found using different sources for a_μ^{exp} and a_μ^{SM} all in the range (25 - 32)$\times 10^{-10}$). Now, assuming any discrepancy is solely due to new physics, and that the current discrepancy is not resolved by results from the new experiments, a rough estimate using Eq. 1.10 sets the scale of these new states at 100 GeV for contributions at $\mathcal{O}(\alpha/\pi)$, or 5 GeV for contributions at $\mathcal{C} = \mathcal{O}((\alpha/\pi)^2)$ such as new fermion loops. Under these assumptions, new states at scales much greater than these estimates would not produce effects of sufficient size to explain the discrepancy. In fact, a BSM fermion of mass roughly the scale of the top quark might only produce a contribution to a_μ of $\mathcal{O}(10^{-12})$, below the sensitivity of current experiments.

Whether or not the discrepancy between experiment and theory remains significant after the publication of new data in the coming years, new constraints will be placed on BSM physics as a result of ongoing muon $g-2$ research. Just as the LHC experiment's excavations of regions of parameter space provide maps of SM theory domination and reduce the hiding places for new physics, so too will the muon $g-2$ contribute in the search. Physics outside the framework of the Standard Model is known to exist; the challenge will be, if significant evidence of its presence is found, to identify which of the vast range of BSM models offers the correct explanation.

In the wider context laid out briefly here, the goal of this thesis is to provide analytic results which serve to sharpen the Lattice QCD-based SM prediction for the LO-HVP contribution to the muon $g-2$, and therefore aid in determining whether or not the new experimental result, upon its release, establishes the presence of BSM physics. The results of the thesis are intended to be of use to those groups studying the HVP in its own right as well as the muon $g-2$. It is ultimately hoped that this work will increase the sphere of knowledge in the field of precision high energy physics research.

Chapter 2

Muon $g-2$ Theoretical Background

The magnetic moment appears through the scattering of a particle by a magnetic field. The muon is a charged particle described by a spinor satisfying the Dirac equation which predicts an interaction between muon spin, $\vec{S} = \frac{1}{2}\vec{\sigma}$, where the $\vec{\sigma}$ are the Pauli matrices, and the magnetic field, B. (In this section we will not add subscripts to the masses since the theory applies equally well to the other leptons, however, unless stated otherwise, one should assume the particle of focus is the muon). In the presence of a magnetic field, the Dirac equation leads to a Hamiltonian in the non-relativistic limit given by [42]

$$H = \frac{q^2}{2m} + V(r) + \frac{e}{2m}\vec{B} \cdot (\vec{L} + g\vec{S}) \tag{2.1}$$

which acts on muon doublets, $|\psi\rangle$, where L is the muon's orbital angular momentum and q^2 is it's momentum squared. The g-factor of the term

$$\frac{e}{2m} g\vec{B} \cdot \vec{S}$$

represents the relative strength of the particle's intrinsic magnetic dipole moment to the strength of the spin-orbit coupling and was predicted by Dirac in the late 1920s to equal 2 [14]. This can easily be shown by taking the non-relativistic limit of the gauged Dirac

equation,

$$(\not{\partial} + ieA_\mu)\psi + m\psi = 0, \tag{2.2}$$

where we use $e > 0$ so that the electric charge of the muon is (-e), to find that it gives the interaction term in the Hamiltonian for a particle in a magnetic field,

$$H_{int} = \frac{e}{m}\vec{B} \cdot \vec{S}. \tag{2.3}$$

Comparing this interaction with the g-factor term in Eq. 2.1 leads one conclude $g = 2$. Although not an obvious fact, it has been firmly established by experimental data dating back to the 1940s that the value of g deviates by a small amount from the Dirac prediction due to quantum corrections. This fact characterises g as a constant different in nature to the lepton U(1) charge quantum number, $Q = -1$, which does not receive quantum corrections.

In quantum field theory (QFT) the scattering of the muon by a magnetic field is represented to lowest order by the diagram

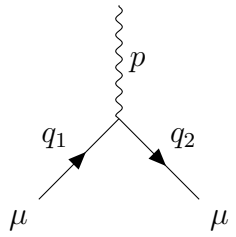

(2.4)

which has a well-known amplitude given in most introductory QFT textbooks[1]

$$i\mathcal{M}_0^\mu = -ie\bar{u}(q_2)\gamma^\mu u(q_1). \tag{2.5}$$

This scattering amplitude can be rewritten using the Gordon identity, which states that

[1]For instance see Chapter 6 of Peskin & Schoeder [43], or Chapter 17 of Schwartz [42]

for any two positive energy solutions of the Dirac equation $u(q_1), u(q_2)$,

$$2m\bar{u}(q_2)\gamma^\mu u(q_1) = \bar{u}(q_1)[(q_1+q_2)^\mu + i\sigma^{\mu\nu}(q_1-q_2)_\nu]u(q_1). \tag{2.6}$$

Labelling the momentum of the photon in the leading order diagram $p^\mu = q_2^\mu - q_1^\mu$, one can then rewrite the lowest-order scattering amplitude as

$$\mathcal{M}_0^\mu = -\frac{e}{2m}\bar{u}(q_2)[(q_1+q_2)^\mu + i\sigma^{\mu\nu}p_\nu]u(q_1). \tag{2.7}$$

The first term in this new expression corresponds to an interaction involving a photon coupled to the momentum of the field as in scalar QED. In the non-relativistic limit (slow-moving particles and static magnetic field) the second term can be identified as the scattering amplitude for a spin-$\frac{1}{2}$ particle that has magnetic moment $\mu = e/2m$ and therefore $g = 2$. Hence we can write g as $4m/e$ times the coefficient of $ip_\nu\bar{u}\sigma^{\mu\nu}u$ and find the quantum corrections to g by studying the loop corrections to this coefficient.

It can be shown [42] that the general expression for the amplitude, valid at any loop order is given by

$$i\mathcal{M}^\mu = (-ie)\bar{u}(q_2)\left[F_1(p^2)\gamma^\mu + \frac{i}{2m}\sigma^{\mu\nu}p_\nu F_2(p^2)\right]u(q_1) \tag{2.8}$$

where F_1 and F_2 are functions of p^2 known as form factors. It is straightforward to see that the amplitude for the leading order diagram, Eq. 2.5, is reproduced by substitution of $F_1 = 1$ and $F_2 = 0$. By comparing this general expression for the amplitude with that of Eq. 2.7 we can see that F_2 has the structure of a magnetic moment. We therefore learn that at the scale of p^2, the value of g is modified by $g = 2 + 2F_2(p^2)$. The theoretical prediction can be compared to measurements of the muon $g-2$ at low energies by taking the non-relativistic limit, where

$$g = 2 + 2F_2(0) \tag{2.9}$$

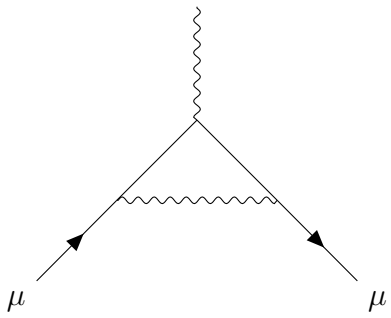

Figure 2.1: The one-loop vertex correction by a single internal photon in muon scattering by an external field.

or

$$F_2(0) = \frac{g-2}{2} = a_\mu. \tag{2.10}$$

Figures 2.1 and 2.2 show the order e^3 one-loop corrections to the scattering amplitude. The diagrams in figure 2.2 represent loop corrections to the external propagators of the lowest- order diagram. There are no finite corrections corresponding to the loop corrections to the external lines since their only effect is a charge renormalisation, producing terms proportional to γ^μ and therefore contributing solely to F_1. Only the diagram of figure 2.1, involving a single internal photon line, produces a finite radiative correction to the muon $g-2$.

The calculation of the one-loop vertex correction was first performed independently by Schwinger, Tomonaga, and Feynman (see Ref. [44] and references therein), leading to the famous result,

$$F_2(0) = \frac{\alpha}{2\pi} \tag{2.11}$$

with α the electromagnetic fine-structure constant. The result for g, including the $\mathcal{O}(\alpha)$ correction, is therefore

$$g = 2 + \frac{\alpha}{\pi} = 2.00232. \tag{2.12}$$

The electron $g-2$ has been predicted theoretically by the successful calculation of the perturbative QED contributions to five loops ($\mathcal{O}(\alpha^5)$, or tenth-order in e) [15].The five-loop

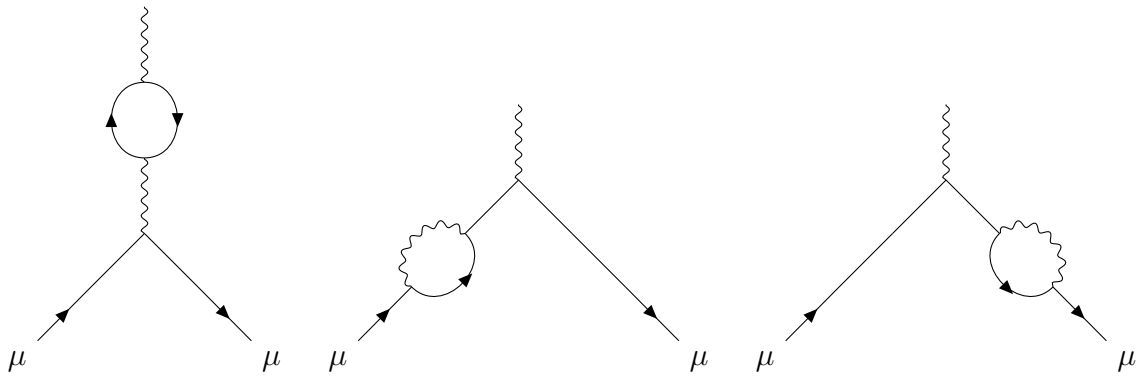

Figure 2.2: Loop corrections to the external propagators in muon scattering.

perturbative result represents the overwhelmingly dominant (>99%) contribution to the Standard Model prediction. It is worth emphasizing the magnitude of the work involved in obtaining this result: while the one-loop, $\mathcal{O}(\alpha)$, result requires evaluating only the single Feynman graph shown above, obtaining the $\mathcal{O}(\alpha^2)$, $\mathcal{O}(\alpha^3)$, $\mathcal{O}(\alpha^4)$, and $\mathcal{O}(\alpha^5)$ contributions requires evaluating 7, 72, 891 and 12672 further Feynmann graphs, respectively.

The corresponding $\mathcal{O}(\alpha^5)$ QED calculation for the muon [32] leads to a current best result of

$$a_\mu^{QED} = 116584718.95(8) \times 10^{-11}. \tag{2.13}$$

With this level of precision for the QED contribution, including electroweak (EW) and hadronic contributions becomes necessary to obtain a reliable Standard Model prediction for a_μ. Figure 2.3 shows the leading-order EW diagrams, which include internal Z and $W^\pm$ boson propagators, however one should note that in general EW corrections may also include the Higgs boson. As pointed out in Ref. [1], the EW contributions are suppressed by at least a factor of

$$\frac{\alpha}{\pi}\frac{m_\mu^2}{m_W^2} \simeq 4 \times 10^{-9}. \tag{2.14}$$

The results of the two-loop EW calculation using a Higgs mass of 125 GeV is presented in Ref. [45]. The value found for a_μ^{EW} by this study was given in the introduction chapter

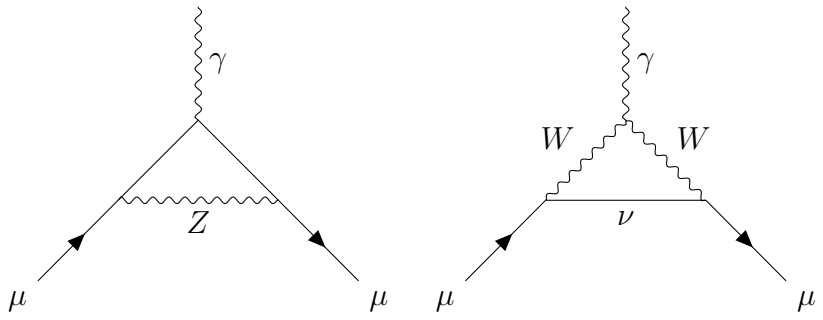

Figure 2.3: The leading order electroweak corrections to the muon $g-2$. Here we use the γ to distinguish between the photon and W, Z boson lines.

of this thesis but we restate the result here,

$$a_\mu^{EW} = 153.6(1.0) \times 10^{-11}. \tag{2.15}$$

The dominant source of error in the EW prediction arises from hadronic physics which enters in the form of fermionic loops. For the full details one can consult the reference given for this result, as well as the review of Ref. [1] and citations therein.

In the next chapter we shall cover the hadronic contributions that enter at $\mathcal{O}(\alpha^2)$.

Chapter 3

Review of Chiral Perturbation Theory

3.1 Introduction to the QCD landscape

Interactions of the strong force are described by the theory of Quantum Chromodynamics (QCD), a local, non-Abelian SU(3) gauge theory with Lagrangian given by

$$\mathcal{L}_{QCD} = -\frac{1}{4}F^a_{\mu\nu}F^{\mu\nu a} + \sum_f \bar{\psi}_f(i\not{D} - m_f)\psi_f \tag{3.1}$$

where the ψ_f are 3-element column vectors in color space, f labels the quark flavour (u, d, c, s, t, b), and

$$F^a_{\mu\nu} = \partial_\mu G^a_\nu - \partial_\nu G^a_\mu - g f^{abc} G^b_\mu G^c_\nu, \tag{3.2}$$

$$D_\mu \psi_f = (\partial_\mu + ig G^a_\mu \frac{\lambda^a}{2})\psi_f. \tag{3.3}$$

Here G^a_μ are the gluon fields, the gauge bosons of the theory, g is the strong coupling, and a is a colour label.

The renormalised strong coupling g exhibits the phenomenon of momentum dependence, referred to as the *running of the coupling constant*. The same is true of the electromagnetic

coupling. Analogous to the QED fine structure constant, in QCD the strong coupling constant is

$$\alpha_s = \frac{g^2}{4\pi}. \tag{3.4}$$

However, the momentum dependence of the QCD and QED couplings differ in a crucial way. The QED coupling α_{EM} is weak at low momentum and becomes stronger as momentum increases. This enables the use of perturbation theory to calculate corrections to QED processes at low energies. QCD is however strongly coupled in the low momentum regime and only grows weak enough to make perturbation theory a useful approach at high energies. The increase of the coupling with decreasing momentum manifests itself in the property of *confinement*. Confinement means that the amount of energy required to separate a system of two quarks inside a hadron increases with the distance between them until eventually the energy becomes large enough to create an additional quark anti-quark pair and the system goes from a single hadron to two hadrons. As a result, quarks and gluons appear in experiments only in bound states. Free quarks and gluons have never been observed [46].

Lattice QCD [47–49] offers an ab initio method of making quantitative predictions of hadronic effects in the non-perturbative regime through evaluation of the QCD path integral in a discretised spacetime. This discretisation takes the form of a set of lattice points at a separation typically denoted a in Euclidean spacetime. Euclidean spacetime results from continuing time in Minkowski space to imaginary values so that the oscillatory energy-dependent exponential factors that characterize time evolution in Minkowski spacetime become exponentially decaying in Euclidean spacetime. The Euclidean squared-momentum, Q^2, is always positive. On the lattice, quark fields live on the lattice sites while gluon fields are represented by *links*,

$$U_\mu(x) = e^{iA_\mu(x+a\hat{\mu}/2)}, \tag{3.5}$$

between sites, where $\hat{\mu}$ is the unit vector in the direction given by μ. U_μ transform co-

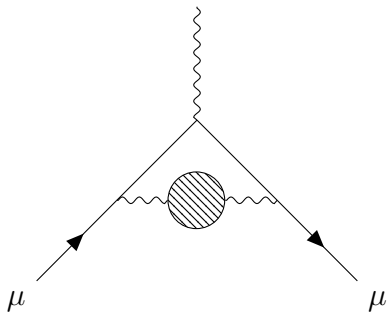

Figure 3.1: The LO-HVP contribution to the muon $g-2$. At leading order in QED, an ingoing muon scatters off a photon, shown here as a wavey line. This diagram displays the addition of a loop correction to that process involving hadronic physics which is represented by the shaded circle.

variantly under SU(3) gauge transformations. This transformation property of the links enables the construction of gauge invariant lattice QCD actions. The continuum is restored in the $a \to 0$ limit.

Lattice QCD (hereafter LQCD) calculations are carried out numerically using large scale Monte Carlo simulations requiring supercomputer access. Therefore progress in this approach is dependent upon the contemporary power of supercomputer resources. Previously, LQCD studies have used unphysical values for parameters such as quark masses, to ease the demand on computing resources and then extrapolated results to make predictions for the physical values. However significant progress has been made in the field over the last few years. Improved numerical algorithms and computing capabilities allowing the use of physical parameter values on finely spaced lattices in the simulations have led to LQCD achieving unprecedented levels of accuracy [50].

Figure 3.1 shows the leading-order $\mathcal{O}(\alpha^2)$ hadronic correction to the lowest-order QED scattering of a muon by an external field as discussed in the previous chapter. The current most precise determination of the hadronic contribution to the muon $g-2$ does not however come from LQCD. Instead QCD dispersion relations [51–53] are used to write the leading-order hadronic a_μ contribution as a weighted integral over experimentally measured cross-

sections for e^+e^- annihilation to hadrons

$$a_\mu^{LO-HVP} = \frac{1}{3}\left(\frac{\alpha}{\pi}\right)^2 \int_{m_\pi^2}^{\infty} ds \frac{K(s)}{s} R^{(0)}(s) \tag{3.6}$$

where $R^{(0)}(s)$ is a ratio which measures the bare cross-section of the $e^+e^- \rightarrow$ hadrons process in units of the point-like $\mu^+\mu^-$ production cross-section, s is the square of the centre of mass energy, and $K(s)$ is an exactly known QED kernel function [54]. This formulation is also described in detail in Chapter 5.1 of Ref. [3]. More precisely, the determination is separated into two regimes dependent upon the energies at which perturbation theory can be successfully applied in QCD. At sufficiently high energies, perturbative QCD can be used to calculate the cross-section ratio and may therefore replace the input from experimental data above a suitable energy cut. By this method the determination is broken down into a non-perturbative part that utilises data and a contribution from the perturbative high energy tail which is numerically very small as a consequence of the form of the QED kernel, which causes the full contribution to be dominated by the low-energy region.

Ref. [55] presents the most recent results for the calculation of the LO-HVP contribution to a_μ by this method. The authors find a result of

$$a_\mu^{LO-HVP} = 693.9(4.0) \times 10^{-10}, \tag{3.7}$$

however the full precision of the newest experimental data cannot be fully exploited due to discrepancies between the data sets in the BABAR [56, 57] and KLOE [58–60] results for the dominant $\pi^+\pi^-$ channel. Other experiments do not match the sub-percent precision of these results and fall in between the BABAR and KLOE values. For these reasons the current discrepancy between the data sets is not able to be resolved.

The alternative approach offered by LQCD is an evaluation of the hadronic loop corrections represented by the shaded circle in Fig. 3.1. The integration is carried out over the magnitude of the loop momenta in Euclidean space, as described in Ref. [61]. In this

formulation the photon propagator can depend only on Q^2, and subsequently so too must the HVP. This fact allows for the HVP to be calculated on the lattice from the Euclidean correlation function of two electromagnetic currents, and then inserted into the one-loop QED diagram without analytical continuation back to Minkowski space or requiring values of Q^2 less than 0, a region inaccessible to LQCD. In recent years LQCD results have become increasingly competitive in terms of their precision compared with the dispersive approach. A review is given by Ref. [26], however one should note that recent updates, such as the most precise determination to-date of isospin-breaking corrections by the ETM collaboration [9] are not included.

The inclusion of isospin-breaking (IB) effects in LQCD calculations, demanded by the target precision of the SM determination, makes it desirable to have an analytical prediction of such effects in order to constrain new results obtained by the various lattice collaborations. IB is inherently included in the dispersive approach through the experimental cross-section data, whereas LQCD calculations include the effects as a small correction at leading-order in $(m_u - m_d)$ to isospin symmetric QCD, $m_u = m_d$. As LQCD studies probe hadronic corrections to $g-2$ physics at this new precision scale it is important that a resource is available which can offer checks on the prediction of the low-energy hadronic behaviour, such as IB effects. The aim of this work is to provide such a resource using an analytical approach known as chiral perturbation theory, the foundations of which are the subject of the remainder of this chapter.

3.2 Effective Field Theory Approach to QCD

A separate approach to low energy QCD is to use effective field theory [62–64]. Effective field theories are useful in cases where there exists a scale separation between the low and high energy degrees of freedom of a theory such as QCD where the up, down and strange (u, d, s) quarks have significantly smaller masses than the charm, top and bottom quarks (c, t, b). Determinations of the quark masses are given in Table 3.1. Due to confinement,

quark masses cannot be measured directly and instead must be measured indirectly through their effects on hadronic properties. Therefore any quantitative results for quark masses are renormalisation scheme dependent. In the mass independent renormalisation scheme used to obtain the results in Table 3.1 [1], the scale separation relevant for the discussion of the effective field theory approach to QCD is the gap between the pseudoscalar meson masses and the mass of the lightest of the heavier resonance states. The c, b and t quarks lie even higher in mass and are therefore also naturally integrated out.

Light quarks		Heavy quarks	
Quark	Mass (MeV/c^2)	Quark	Mass (MeV/c^2)
up	$2.2^{+0.6}_{-0.4}$	charm	1280 ± 30
down	$4.7^{+0.5}_{-0.4}$	bottom	4180^{+40}_{-30}
strange	96^{+8}_{-4}	top	173100 ± 600

Table 3.1: Quark masses as given in the review by the Particle Data Group (PDG) [1]. The mass values in MeV of the up, down and strange quarks presented are estimates of current-quark masses in the mass-independent $\overline{\text{MS}}$ subtraction scheme at a scale μ =2 GeV. The values of the charm and bottom quark masses are also given in the $\overline{\text{MS}}$ scheme. Lastly, the top quark mass is based on direct measurements of the cross-sections for the production of top-anti-top pairs. The mass of the top quark is its most precisely studied property and has been measured by all four Tevatron (CDF, D$\emptyset$) and LHC experiments (ATLAS, CMS) in the lepton+jets, the dilepton, and the all-jets channels. A complete discussion of the definition of the top quark mass is presented in Ref. [1] in the review 'The Top Quark'.

Perturbative calculations in QFT involve summing over the contributions of all states at all momenta. However, from Heisenberg's uncertainty principle, high momentum effects manifest themselves to us as short distance phenomena. In a low-energy effective Lagrangian, only the low-energy degrees of freedom are included explicitly, and the effects of the high-energy (short distance) degrees of freedom that have been "integrated out", are incorporated through the presence of local terms whose coefficients are in principle determined by the high energy physics in the underlying fundamental theory. Low energy (long distance) effects, produced by the low energy degrees of freedom that can propagate long distances, are dealt with through the low-energy degrees of freedom explicitly included in the effective Lagrangian. The identification of the low and high energy (long and short

distance) effects in a theory is the basis of effective field theory. The loop corrections to low energy processes in QFT still involve the high energy effects because one is required to integrate over all loop momenta, however the process of renormalisation allows the high energy effects to be absorbed into the renormalised coefficients of the local effective Lagrangian. This is of course necessary since relying on a given theory to give realistic results at arbitrarily high momentum is to extend its domain of validity beyond what has been verified experimentally.

In the path integral formulation of QFT, a theory containing light, ϕ, and heavy, Φ, fields is described by the functional integral

$$Z = \int \mathcal{D}\phi \mathcal{D}\Phi \exp\left(i \int d^4x \mathcal{L}(\phi, \Phi) \right). \tag{3.8}$$

Integrating out the high energy fields (see chapters 11 and 12 of Ref. [43]) produces a description of a non-local effective Lagrangian with effective interactions involving only the light degrees of freedom,

$$Z = \int \mathcal{D}\phi \exp\left(i \int d^4x \mathcal{L}_{eff}(\phi) \right). \tag{3.9}$$

The effective theory is only valid below the scale at which the heavy degrees of freedom were integrated out. Yet the virtual effects of the heavy fields are included in theory in the form of low energy coefficients (LECs) of terms to all orders in the effective theory. The new effective Lagrangian can be used to calculate correlation functions involving the light fields, ϕ, or to compute S-matrix elements.

An important feature of effective field theories (EFTs) is that they offer a systematic expansion in some small power counting parameter, δ. Therefore the method by which one can compute higher order corrections is well-defined: hypothetically one could perform expansions to some order n at which the associated error is given by δ^{n+1} and hence, in principle, any desired level of error could be achieved by expanding to sufficient order.

In practice this procedure is limited by multiple factors including the difficulty of the ensuing higher order diagrams of the expansion. Still, EFTs have proven very useful for the computation of measurable quantities without input from the full underlying theory, particularly in the case of QCD. The low-energy EFT of QCD is *chiral perturbation theory* (ChPT) which has provided results in excellent agreement with experiments [65–67].

The power of EFTs lies in identifying topics in particle physics which benefit from an EFT approach. The muon $g-2$ is one such topic. The hadronic contribution to the muon $g-2$ is dominated by the low momentum squared (low-q^2) regime due to the form of the electromagnetic kernel $f(q^2)$ [61] which diverges as $q^2 \to 0$. A low-energy QCD prescription then has a good chance of providing a reliable means of computing the LO-HVP corrections to the muon $g-2$ since one would expect low energy effects to be enhanced by this behavior of $f(q^2)$.

The question of whether the largest hadronic contributions come from the region of ChPT validity is worthy of investigation. LQCD studies will benefit greatly from analytical constraints at low-energies, particularly with the anticipated release of a new experimental determination of a_μ at improved precision levels. The results obtained by lattice calculations are set to play an integral role in analysing whether the new results can be explained by the SM. Hence if a ChPT analysis at the current possible order in the perturbative expansion can be proven capable of describing the dominant hadronic processes contributing to $g-2$ physics, then it is hoped that ChPT results may complement the studies which will play a critical role in determining if the new experimental data can be explained by the SM.

The purpose of the remainder of this chapter is to review the formulation of ChPT in order to elucidate its main features underlying the vacuum polarisation calculation that forms the basis of the research carried out in this thesis.

3.3 The Chiral Symmetry of QCD

Chirality (or 'handedness') is a property of fermions related to the relative alignment of their spin and momentum vectors. A fermion with positive helicity, meaning that its spin and momentum are aligned, is spinning in the direction given by the right hand rule. Conversely a fermion with negative helicity, or anti-alignment of spin and momentum, spins according to the left hand rule. For massless fermions this coincides exactly with chirality. If $\psi(x)$ is a solution of the Dirac equation for a massless free fermion,

$$i\partial\!\!\!/\psi = 0 \tag{3.10}$$

then another solution can be found by multiplying by γ_5 ($= i\gamma^0\gamma^1\gamma^2\gamma^3$, where γ_i, ($i = 0, 1, 2, 3$) are the Dirac matrices) and using

$$\{\gamma_5, \gamma_\mu\} = 0 \tag{3.11}$$

to find

$$i\partial\!\!\!/\gamma_5\psi = 0. \tag{3.12}$$

Alternatively we can write a pair of linearly independent solutions

$$\psi_L = \frac{1}{2}(\mathbb{1} - \gamma_5)\psi\,, \qquad \psi_R = \frac{1}{2}(\mathbb{1} + \gamma_5)\psi \tag{3.13}$$

where $\psi_{L,R}$ have definite chirality. One can then define chirality projection operators $\Gamma_{L,R} = (1 \mp \gamma_5)/2$ so that the left and right chiral components can be written as

$$\psi_L = \Gamma_L\psi\,, \qquad \psi_R = \Gamma_R\psi. \tag{3.14}$$

One may then note that the chiral components are eigenfunctions of the γ_5 matrix,

$$\gamma_5 \psi_L = -\psi_L \tag{3.15}$$

$$\gamma_5 \psi_R = +\psi_R. \tag{3.16}$$

The property of chirality in the massless limit as defined by γ_5 is Lorentz invariant and therefore chirality is a natural label to give to massless fermions.

Chiral symmetry can be identified in the Lagrangian for massless fermions,

$$\mathcal{L} = i\bar{\psi}\partial\!\!\!/\psi \tag{3.17}$$

by using $\psi = \psi_L + \psi_R$ to write

$$\mathcal{L} = i\bar{\psi}_L\partial\!\!\!/\psi_L + i\bar{\psi}_R\partial\!\!\!/\psi_R \tag{3.18}$$

$$= \mathcal{L}_L + \mathcal{L}_R. \tag{3.19}$$

$\mathcal{L}_{L,R}$ are invariant under global chiral phase transformations

$$\psi_L \to \exp(-i\theta_L)\psi_L, \tag{3.20}$$

$$\psi_R \to \exp(-i\theta_R)\psi_R. \tag{3.21}$$

This is a chiral symmetry since the transformations act independently on the fields with definite chirality.

Massive fermions do not share this symmetry since the mass term in the Lagrangian,

$$\mathcal{L}_m = \bar{\psi} m \psi \tag{3.22}$$

is not invariant under the chiral transformations and therefore explicitly breaks the chiral symmetry.

If we consider the Lagrangian of QCD, given by Eq. 3.1, in the massless limit,

$$\mathcal{L}_{QCD} = -\frac{1}{4}F^a_{\mu\nu}F^{\mu\nu a} + \sum_f \bar{q}_f i \not{D} q_f \tag{3.23}$$

we find, decomposing the quark fields into their chiral components by $q_f = q^f_L + q^f_R$, that this Lagrangian has the chiral symmetries described above. By Noether's theorem, the existence of these symmetries implies the existence of associated conserved currents, J_μ. The conservation equation

$$\partial_\mu J^\mu = 0 \tag{3.24}$$

ensures that each such current has an associated classical time-independent charge Q.

Consider a generic infinitesimal transformation with fields transforming under infinitesimal transformations parametrised by ϵ as $\phi \to \phi + \epsilon\delta\phi$. If such a transformation leaves the action invariant then the conserved Noether current is defined by

$$J^\mu(x) \equiv \frac{\delta\mathcal{L}}{\partial(\partial^\mu\phi)}\delta\phi. \tag{3.25}$$

The QCD Lagrangian is invariant under the vector transformations

$$q \to e^{-i\epsilon^V_a T^a} q \approx \left(1 - i\epsilon^V_a T^a\right) q \tag{3.26}$$

where T^a are the generators of the corresponding continuous symmetry group on the space of the fields, and ϵ^V_a are the parameters of the infinitesimal versions of these transformations. Therefore by identifying $\delta\phi = -iT^a q$, the corresponding Noether currents can be

constructed, using the fact that

$$\begin{aligned}\frac{\partial \mathcal{L}_{QCD}}{\partial(\partial_\mu q)} &= \frac{\partial}{\partial(\partial_\mu q)}(\bar{q} i \not{D} q) \\ &= i\bar{q}\gamma^\nu \frac{\partial(\partial_\nu q)}{\partial(\partial_\mu q)} \\ &= i\bar{q}\gamma^\mu . \end{aligned} \tag{3.27}$$

From the discussion above it follows that the QCD Lagrangian for n_ℓ massless quarks is also invariant under the independent left and right chiral $\mathrm{U}(n_\ell)$ transformations, and hence has a classical $\mathrm{U}_L(n_\ell)\times\mathrm{U}_R(n_\ell)$ symmetry. The corresponding conserved right and left handed currents, R^a_μ and L^a_μ, respectively, are obtained by the usual construction

$$\begin{aligned} R^a_\mu &= \frac{\partial \mathcal{L}_{QCD}}{\partial(\partial_\mu q_R)}\delta q_R \\ &= i\bar{q}_R\gamma^\mu(-iT^a q_R) = \bar{q}_R\gamma^\mu T^a q_R \end{aligned} \tag{3.28}$$

$$\begin{aligned} L^a_\mu &= \frac{\partial \mathcal{L}_{QCD}}{\partial(\partial_\mu q_L)}\delta q_L \\ &= i\bar{q}_L\gamma^\mu(-iT^a q_L) = \bar{q}_L\gamma^\mu T^a q_L \ . \end{aligned} \tag{3.29}$$

Their sum is the corresponding conserved vector current

$$\begin{aligned} V^a_\mu &= R^a_\mu + L^a_\mu \\ &= \bar{q}\gamma^\mu T^a q \ . \end{aligned} \tag{3.30}$$

For the axial current the method is repeated using the axial transformations which act

differently on the left and right chiral states,

$$q_L = e^{-i\epsilon_a^A T^a \gamma_5} q_L \tag{3.31}$$

$$q_R = e^{-i\epsilon_a^A T^a \gamma_5} q_R. \tag{3.32}$$

The result is $A_\mu^a = R_\mu^a - L_\mu^a$, or

$$A_\mu^a = \bar{q}\gamma_\mu\gamma_5 T^a q. \tag{3.33}$$

The vector and axial transformations are simply linear combinations of the L and R transformations.

The group of symmetries generally referred to as the chiral symmetry group of QCD is the subgroup $\mathrm{SU}(N_f)_L \times \mathrm{SU}(N_f)_R$ of the classical chiral symmetry group $\mathrm{U}(N_f) \times \mathrm{U}(N_f)$, where N_f is the number of light quark flavours. The aforementioned scale separation between the light and heavy quarks can be utilised by making the approximation that the light quarks (u, d, s) are massless and treating their masses as perturbations about this *chiral* limit. QCD in this massless, $N_f = 3$ approximation has an $\mathrm{SU}(3)_L \times \mathrm{SU}(3)_R$ chiral symmetry. The T^a appearing in the conserved currents above are then the SU(3) generators $T_a = \lambda_a/2$, where λ_a are the 3×3 Gell-Mann matrices, normalised by

$$\mathrm{Tr}(\lambda_a \lambda_b) = 2\delta^{ab}. \tag{3.34}$$

The vector and axial currents are then given by

$$V_\mu^a = \bar{q}\gamma_\mu \frac{\lambda^a}{2} q \tag{3.35}$$

$$A_\mu^a = \bar{q}\gamma_\mu\gamma_5 \frac{\lambda^a}{2} q. \tag{3.36}$$

where V_μ^a is a Lorentz vector, and A_μ^a is a Lorentz pseudovector with corresponding scalar

and pseudoscalar charges respectively, having different transformations under parity,

$$Q_V^a \to Q_V^a\,, \qquad Q_A^a \to -Q_A^a. \tag{3.37}$$

3.4 Spontaneous Breaking of Chiral Symmetry

If $|\psi\rangle$ is an eigenstate of the QCD Hamiltonian, H_{QCD}, in the chiral limit,

$$H_{QCD}|\psi\rangle = E|\psi\rangle \tag{3.38}$$

then, for a conserved vector or axial charge Q, the commutativity of Q with H can be used to show

$$H_{QCD}[Q|\psi\rangle] = E(Q|\psi\rangle). \tag{3.39}$$

Therefore the vector and axial charges give rise to states with the same energy but opposite parity. These opposite parity states of equal energy are not realised in the form of pairs of opposite parity *single-particle* states in nature; the observed spectrum of QCD degrees of freedom reveals that the $J^P = 0^-$ pseudoscalar mesons are considerably lighter than the $J^P = 0^+$ scalar mesons [1]. This does not mean that states of opposite parity but approximately even mass do not exist, for example the nucleon and nucleon plus pion states display this property due to the relative smallness of the pion mass.

This paradox is resolved by the phenomenon of spontaneous symmetry breaking. This can be described by considering a Lagrangian in possession of a particular symmetry. There are two possibilities for the ground state of the system: either the ground state can be non-degenerate and is therefore a unique state possessing the same symmetry as the Lagrangian, or it can be degenerate meaning that there is no unique state which represents the ground state. In the case of having no unique ground state, if we arbitrarily choose one out of the many degenerate states to be the ground state then we find that this chosen state does not share the symmetry of the Lagrangian. The process by which an asymmetric

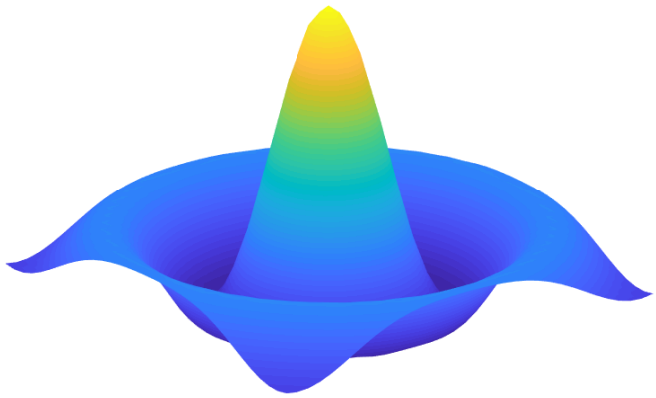

Figure 3.2: A Mexican hat potential illustrating a degenerate ground state shown here as the minimum of the potential.

ground state is obtained is called spontaneous symmetry breaking. Perturbations about the asymmetric ground state will produce excited states which also feature the asymmetry.

The ground state of a QFT is the vacuum. Therefore spontaneous symmetry breaking applies in QFTs where the vacuum is non-degenerate. In the case of the chiral $\mathrm{SU}(3)_L \times \mathrm{SU}(3)_R$ symmetry, the action of the vector charges on the vacuum leave it invariant, but the axial charges do not,

$$Q_V^a|0\rangle = 0 \tag{3.40}$$

$$Q_A^a|0\rangle \neq 0. \tag{3.41}$$

Goldstone's theorem [68] tells us that the spontaneous breaking of a continuous symmetry corresponds to the existence of a massless particle, known as a Goldstone boson, for each broken generator. Q_i is a broken generator if $Q_i|0\rangle \neq 0$. Assume that there is a symmetry

group with generators Q_k such that $\delta\phi = i\epsilon^k Q_k \phi$, and that the fields ϕ have vacuum expectation values, $\mathcal{V}$.

$$\phi = \begin{pmatrix} \phi_1 \\ \vdots \\ \phi_N \end{pmatrix}, \qquad \mathcal{V} = \begin{pmatrix} \mathcal{V}_1 \\ \vdots \\ \mathcal{V}_N \end{pmatrix} \tag{3.42}$$

$\mathcal{V}$ must be a minimum of the potential $V(\phi)$ and must therefore satisfy the conditions:

$$\frac{\partial V(\mathcal{V})}{\partial \phi_j} = 0 \tag{3.43}$$

$$\frac{\partial^2 V(\mathcal{V})}{\partial \phi_j \partial \phi_k} \geq 0 \tag{3.44}$$

If Q_k is a broken generator then $Q_k \mathcal{V} \neq 0$. We want to perform an expansion of the Lagrangian about the vacuum and to do this we redefine the fields in terms of their vacuum expectation values,

$$\phi_k = \mathcal{V}_k + \phi'_k \tag{3.45}$$

which means that the Lagrangian can be written in terms of the shifted fields ϕ',

$$\mathcal{L}(\phi') = \partial_\mu \phi'_k \partial^\mu \phi'_k - V(\mathcal{V}) - \frac{1}{2}\Big(\frac{\partial^2 V(\mathcal{V})}{\partial \phi_j \partial \phi_k}\Big)\phi'_j \phi'_k + ... \tag{3.46}$$

The coefficient of the quadratic term in this expansion is the mass squared matrix of the fields

$$\frac{\partial^2 V(\mathcal{V})}{\partial \phi_a \partial \phi_b} = m^2_{ab} \tag{3.47}$$

which is a symmetric matrix with eigenvalues that give the masses of the fields. For Goldstone's theorem, we must show that every continuous symmetry of the Lagrangian that is not also a symmetry of the vacuum expectation, $\mathcal{V}$, must have a mass matrix

eigenvalue of zero.

$$\delta V = V(\phi + \delta\phi) - V(\phi) \tag{3.48}$$

$$= V(\phi) + \frac{\partial V(\phi)}{\partial \phi_i}\delta\phi_i - V(\phi) = \frac{\partial V(\phi)}{\partial \phi_i}\delta\phi_i \tag{3.49}$$

$$= i\frac{\partial V(\phi)}{\partial \phi_i}(\epsilon_k Q^k)_{ij}\phi_j \tag{3.50}$$

$$= 0 \tag{3.51}$$

where in the last line we used the fact that the transformation is a symmetry of V. Now, differentiating the whole expression with respect to ϕ_m,

$$\frac{\partial^2 V(\phi)}{\partial \phi_i \partial \phi_m} Q^k_{ij}\phi_j + \frac{\partial V(\phi)}{\partial \phi_i} Q^k_{ij}\frac{\partial \phi_j}{\partial \phi_m} = 0 \tag{3.52}$$

$$\Rightarrow \frac{\partial^2 V(\phi)}{\partial \phi_i \partial \phi_m} Q^k_{ij}\phi_j + \frac{\partial V(\phi)}{\partial \phi_i} Q^k_{im} = 0 \tag{3.53}$$

Finally we set $\phi = \mathcal{V}$ and use the conditions of minima to find

$$\frac{\partial^2 V(\mathcal{V})}{\partial \phi_i \partial \phi_m} Q^k_{ij}\mathcal{V}_j = 0 \tag{3.54}$$

$$\Rightarrow m^2_{im} Q^k_{ij}\mathcal{V}_j = 0 \tag{3.55}$$

Therefore $Q^k\mathcal{V}$ is an eigenvector of the mass-squared matrix with eigenvalue zero.

In summary, if a transformation does not leave the vacuum invariant, there must exist a massless particle. Or, alternatively, for every broken generator there is a non-trivial independent eigenvector of the mass squared matrix with an eigenvalue of zero. Since SU(N) has $N^2 - 1$ generators, the spontaneous breaking of the axial symmetries means that if the number of massless quarks is 2, there are $2^2 - 1 = 3$ massless pseudoscalar particles, while if the number of massless quarks is 3, there are $3^2 - 1 = 8$ massless pseudoscalar particles.

In the limit that the u, d and s quarks were all massless, the spontaneous break-

Pseudoscalar ($J^P = 0^-$) Meson Mass summary table	
Meson	Mass (MeV)
$\pi^{\pm}$	139.57061 ± 0.00024
π^0	134.9770 ± 0.0005
$K^{\pm}$	493.677 ± 0.016
$K^0, \bar{K}^0$	497.611 ± 0.013
η	547.862 ± 0.017

Table 3.2: All values from 2018 Particle Data Group Review [1].

ing of the 8 axial SU(3) charges in QCD would give rise to eight pseudoscalar mesons, $\pi^{\pm}, \pi^0, K^{\pm}, K^0, \bar{K}^0, \eta$, all having zero mass. Since these mesons are observed to have non-zero masses in nature, it follows that the SU(3) chiral symmetry is not exact, and that the u, d and s masses are non-zero. The fact that the masses of these 8 pseudoscalar states are significantly smaller than those of all other hadrons, however, indicates that the SU(3) chiral symmetry is a good approximate symmetry of QCD, and hence that the light-quark masses can be treated as small perturbations about the chiral limit.

3.5 Construction of the Effective Lagrangian

In order to see how the 'Goldstone bosons' are represented in the chiral Lagrangian we can study their transformation properties under chiral transformations in the language of group theory. Consider G to be the group of $\mathrm{SU}(3)_L \times \mathrm{SU}(3)_R$ transformations with a representation provided by the Goldstone boson fields, ϕ,

$$\phi \to \phi' = F(g, \phi), \quad g \in G. \tag{3.56}$$

Furthermore there is a subgroup, H, of G containing transformations under $\mathrm{SU}(3)_V$ which leave the vacuum of the theory invariant,

$$f(h, 0) = 0 \quad \forall h \in H. \tag{3.57}$$

If g_1 and g_2 are elements in the same coset of H, so that $g_1^{-1}g_2 \in H$ or $g_2 = g_1 h$ for some $h \in H$ then

$$f(g_2, 0) = f(g_1 h, 0) = f(g_1, f(h, 0)) = f(g_1, 0) \ . \tag{3.58}$$

and we can consider the Goldstone bosons to live on the coset space G/H. The number of Goldstone bosons is thus equal to the dimension of the coset space. By making an arbitrary choice of representatives in the coset space, the Goldstone bosons can be chosen to provide an exponential parameterisation,

$$U = \exp\left(\frac{i\lambda_a \phi_a}{f}\right) \tag{3.59}$$

of a matrix-valued field U, transforming under generic $\mathrm{SU}(3)_{L,R}$ L and R as

$$U(x) \to U'(x) = LU(x)R^\dagger \ . \tag{3.60}$$

The ϕ_a here are the pseudoscalar octet fields, and [1]

$$\lambda_a \phi_a = \begin{pmatrix} \phi_3 + \frac{\phi_8}{\sqrt{3}} & \sqrt{2}\pi^+ & \sqrt{2}K^+ \\ \sqrt{2}\pi^- & -\phi_3 + \frac{\phi_8}{\sqrt{3}} & \sqrt{2}K^0 \\ \sqrt{2}K^- & \sqrt{2}\bar{K}^0 & -\frac{2\phi_8}{\sqrt{3}} \end{pmatrix} . \tag{3.61}$$

f is a dimensionful constant which turns out to be equal to the pseudoscalar decay constant in the chiral limit.

The Lagrangian of ChPT, in the absence of quark masses and external fields, is written in terms of the matrix valued field U and its derivatives,

$$\mathcal{L}_{eff} = \mathcal{L}_{eff}(U, \partial U, \partial^2 U, ...). \tag{3.62}$$

[1] The expression given here for $\lambda_a \phi_a$ is written in terms of fields with definite isospin and hypercharge. In the presence of isospin breaking the physical π^0 field differs from the isospin-pure field ϕ_3 by a small isospin-breaking admixture proportion to ϕ_8. Similarly, the physical η field differs from ϕ_8 by a small isospin-breaking admixture proportional to ϕ_3. The relations between the ϕ_a and the physical fields are listed in the appendix.

Chiral power counting is used to arrange the terms in the Lagrangian in order of their chiral power. In the chiral limit this is just the number of derivatives, or, equivalently, the number of momentum factors, and limiting the chiral order corresponds to making a small-momentum expansion. When quark masses are included, these have, for consistency, to be counted as second order in the chiral expansion, for the reason discussed below. The effective Lagrangian is constructed to have the same symmetries as full QCD, those being C, P, T, Lorentz invariance and additional chiral $\mathrm{SU}(3)_L \times \mathrm{SU}(3)_R$. As the Lagrangian is a Lorentz scalar only terms with even chiral powers can appear. The immediate consequence of this is the vanishing of the Lagrangian at zeroth order since the only possible term is a function of $UU^\dagger$ and since U is unitary the result is simply a disposable constant. Therefore, using subscripts to indicate the chiral power, we have

$$\mathcal{L}_{eff} = \mathcal{L}_2 + \mathcal{L}_4 + \mathcal{L}_6 + \ldots \ . \tag{3.63}$$

At leading order in the chiral expansion there is only one term,

$$\mathcal{L}_2 = c_1 \langle \partial_\mu U \partial^\mu U^\dagger \rangle \tag{3.64}$$

where we have chosen the convention of using angle brackets to mean the trace $\langle ... \rangle = \mathrm{Tr}(...)$. The trace is used to construct invariants under the chiral symmetry: if two objects A and B transform as $A \to LAR^\dagger$ and $B \to LBR^\dagger$, invariants are obtained by taking the trace of products of the type $AB^\dagger$.

The constant c_1 is a LEC which is fixed by expanding U in powers of the Goldstone fields,

$$U = 1 + i\frac{\lambda \cdot \phi}{f} - \frac{1}{2}\Big(\frac{\lambda \cdot \phi}{f}\Big)^2 - \frac{i}{6}\Big(\frac{\lambda \cdot \phi}{f}\Big)^3 + \mathcal{O}(\phi^4) \tag{3.65}$$

and requiring the kinetic term to have standard canonical form,

$$\mathcal{L}_2 \sim \frac{1}{2}\partial_\mu \phi^a \partial^\mu \phi^a, \tag{3.66}$$

from which it follows that

$$c_1 = \frac{f^2}{4} \tag{3.67}$$

The leading order term involving derivatives of the Goldstone bosons is thus

$$\mathcal{L}_2 = \frac{f^2}{4}\langle \partial_\mu U \partial^\mu U^\dagger \rangle. \tag{3.68}$$

From the form of the axial current of chiral symmetry, it can be shown [2], as previously mentioned, that f is equal to the GB decay constant in the chiral limit,

$$\langle 0|A^a_\mu(0)|\phi^b(p)\rangle = ip_\mu \delta^{ab} f_a. \tag{3.69}$$

External scalar, pseudoscalar, vector, and axial sources are included in the Lagrangian by writing down terms involving these sources which have the same symmetry breaking patterns as in full QCD [2]. The scalar, s, and pseudoscalar p sources are conventionally introduced through the quantity

$$\chi = 2B_0(s - ip) \tag{3.70}$$

where B_0 is a constant related to the quark condensate in the chiral limit,

$$\langle 0|\bar{q}q|0\rangle = -f^2 B_0 + \mathcal{O}(m_q), \tag{3.71}$$

where $q = u, d, s$ [66]. The effect of this term on the masses of the pseudoscalar mesons will be discussed in the next section. The vector and axial sources are defined through linear combinations of left- and right-handed sources, l_μ and r_μ. These sources enter into the Lagrangian via the associated covariant derivatives and external field field-strength tensors. For any object, A which transforms in the same manner as U under $\mathrm{SU}(3)_{L,R}$, as in Eq. 3.60, the covariant derivative is defined in terms of the left- and right-handed

sources, l_μ and r_μ respectively, as

$$D_\mu A \equiv \partial_\mu A - i r_\mu A + i A l_\mu. \tag{3.72}$$

Furthermore, due to the fact that the chiral Lagrangian contains arbitrarily high powers of derivatives we also require the field strength tensors $L_{\mu\nu}$ and $R_{\mu\nu}$,

$$L_{\mu\nu} = \partial_\mu l_\nu - \partial_\nu l_\mu - i[l_\mu, l_\nu], \tag{3.73}$$

$$R_{\mu\nu} = \partial_\mu r_\nu - \partial_\nu r_\mu - i[r_\mu, r_\nu] \tag{3.74}$$

which are traceless since $\langle l_\mu \rangle = \langle r_\mu \rangle = 0$. The complete form of the most general, locally invariant, effective Lagrangian at lowest order in the chiral series, $\mathcal{L}_2$ is given by [66]

$$\mathcal{L}_2 = \frac{f^2}{4}\langle D_\mu U D^\mu U^\dagger \rangle + \frac{f^2}{4}\langle \chi U^\dagger + U \chi^\dagger \rangle. \tag{3.75}$$

3.6 Coupling to External Vector Currents and Chiral Ordering

The description of QCD plus its coupling to electromagnetism is given by a Lagrangian with external sources, specifically in this case with only external vector sources $v_\mu = eQA_\mu$ and external scalar source $s = \mathcal{M}$ where e is the electromagnetic charge of the proton, Q is the quark charge matrix,

$$Q = \begin{pmatrix} 2/3 & 0 & 0 \\ 0 & -1/3 & 0 \\ 0 & 0 & -1/3 \end{pmatrix} \tag{3.76}$$

A_μ is the electromagnetic field, and $\mathcal{M}$ is the quark mass matrix[2]

$$\mathcal{M} = \begin{pmatrix} m_u & 0 & 0 \\ 0 & m_d & 0 \\ 0 & 0 & m_s \end{pmatrix}. \tag{3.78}$$

The axial and pseudoscalar sources in this case can be set equal to 0. With only vector sources, the covariant derivative is

$$D_\mu U \equiv \partial_\mu U - i[v_\mu, U]. \tag{3.79}$$

Since the sources enter in the same way as the standard derivative, they are counted as $\mathcal{O}(q)$ in the chiral counting. The vector field strength tensor, $F^{\mu\nu}$, is defined by

$$F_{\mu\nu} = \partial_\mu v_\nu - \partial_\nu v_\mu - [v_\mu, v_\nu] \tag{3.80}$$

and hence is to be treated, for consistency, as $\mathcal{O}(q^2)$ in the chiral counting. As for the chiral order of the external scalar source terms, in the absence of a pseudoscalar source, $p = 0$ and setting the scalar source equal to the quark mass matrix $s = \mathcal{M}$, we have

$$\chi = 2B_0\mathcal{M} \tag{3.81}$$

and the second term in the lowest order effective chiral Lagrangian, Eq. 3.75, becomes

$$\frac{f^2}{2}B_0\langle\mathcal{M}(U + U^\dagger)\rangle = (m_u + m_d + m_s)B_0 f^2 - \frac{1}{2}B_0\langle\mathcal{M}\phi^2\rangle + \mathcal{O}(\phi^4) \tag{3.82}$$

[2]For the purposes of this thesis, it is relevant to note that, in general, the QCD operator for the u and d masses, $m_u\bar{u}u + m_d\bar{d}d$, can be re-written in the form

$$\left(\frac{m_u + m_d}{2}\right)(\bar{u}u + \bar{d}d) + \left(\frac{m_u - m_d}{2}\right)(\bar{u}u - \bar{d}d). \tag{3.77}$$

The first term, which is proportional to the average of the u and d masses, $\hat{m} = (m_u + m_d)/2$, has isospin I=0, while the second, which survives only when $m_u \neq m_d$, has isospin I=1. It is this second term which is responsible for SIB.

where U and $U^\dagger$ have been expanded in powers of ϕ, the pseudoscalar octet matrix. The second term, being quadratic in the pseudoscalar fields, determines the masses of the these fields. Performing the trace, one finds

$$\begin{aligned}\langle \mathcal{M}\phi^2 \rangle =& 2(m_u + m_d)\pi^+\pi^- + 2(m_u + m_s)K^+K^- + 2(m_d + m_s)K^0\bar{K}^0 \\ &+ (m_u + m_d)\phi_3\phi_3 + \frac{2}{\sqrt{3}}(m_u - m_d)\phi_3\phi_8 + \frac{m_u + m_d + 4m_s}{3}\phi_8\phi_8. \end{aligned} \tag{3.83}$$

From this expression one can read off the lowest-order expressions for the masses of the pseudoscalar mesons as

$$m^2_{\phi_3} = B_0(m_u + m_d) \tag{3.84}$$

$$m^2_{\phi_8} = \frac{B_0}{3}(m_u + m_d + 4m_s) \tag{3.85}$$

$$m^2_{\pi^\pm} = B_0(m_u + m_d) \tag{3.86}$$

$$m^2_{K^\pm} = B_0(m_u + m_s) \tag{3.87}$$

$$m^2_{K^0} = B_0(m_d + m_s) \tag{3.88}$$

$$m^2_{\phi_3\phi_8} = \frac{B_0}{\sqrt{3}}(m_u - m_d). \tag{3.89}$$

In the isospin limit, $m_u = m_d$, $m^2_{\phi_3}$ becomes $m^2_{\pi^0}$, $m^2_{\phi_8}$ becomes m^2_η and the off-diagonal $\phi_3 - \phi_8$ element of the mass matrix disappears, i.e., there is no $\pi^0 - \eta$ mixing. The meson squared masses are hence proportional to the quark masses and therefore to the elements of χ. To satisfy the on-shell condition $m^2_\phi = p^\phi_\mu p^\mu_\phi$, one must, for consistency, count χ as $\mathcal{O}(q^2)$ in the chiral expansion. Hence the lowest-order Lagrangian at $\mathcal{O}(q^2)$, with $p = 0$ and $s = \mathcal{M}$, is given by

$$\mathcal{L}_2 = \frac{f^2}{4}\langle D_\mu U D^\mu U^\dagger \rangle + \frac{f^2}{2}B_0\langle \mathcal{M}(U^\dagger + U)\rangle. \tag{3.90}$$

A summary of the chiral order of the elements from which the effective Lagrangian is composed is given in Table 3.3. For a set of instructive examples of the application of

Element	Chiral Order
U	$\mathcal{O}(q^0)$
$D_\mu U$	$\mathcal{O}(q)$
$r_\mu, l_\mu, a_\mu, v_\mu$	$\mathcal{O}(q)$
$F_{\mu\nu}, L_{\mu\nu}, R_{\mu\nu}$	$\mathcal{O}(q^2)$
χ	$\mathcal{O}(q^2)$

Table 3.3: Summary of Lagrangian elements and their order in the counting scheme of ChPT [2].

ChPT at lowest-order see the discussion of pion decay, pion-pion scattering, and Compton scattering presented in Chapter 3 of Ref. [2].

3.7 Chiral Perturbation Theory Beyond Leading-Order

The effective Lagrangian contains, in principle, an infinite number of terms with an infinite number of free coefficient parameters to be determined from experiment. When it comes to calculating loop processes in ChPT, the arbitrarily high orders of derivatives in the effective Lagrangian would require the infinite set of coefficients to be renormalised. The chiral Lagrangian is therefore not a renormalisable theory. The solution to this problem was found by Weinberg [67] who in 1979 laid out a systematic approach to calculating corrections beyond tree-level. The argument goes that for the Goldstone boson sector the higher order terms in the effective Lagrangian do not renormalise the coefficients appearing at lower order in the chiral expansion if one uses a suitable regularisation scheme, such as dimensional regularisation (see Ref. [43] for details). Furthermore, to any fixed order in the chiral expansion the divergences will be generated at higher order and theory acts as though it is renormalisable. The successful renormalisation of the finite number of lower-order coefficients is not dependent on the renormalisation of the infinite number of higher-order ones.

Consider a diagram where the number of loops is given by L. The chiral order (or

dimension), D, of the diagram is given by [67],

$$D = 2 + 2L + \sum_k (k-2)N_k \tag{3.91}$$

where N_k is the number of vertices of $\mathcal{O}(q^k)$. Vertices from $\mathcal{L}_2$ do not change the chiral dimension, whereas higher order vertices increase D. One also finds that, in terms of the effect upon D, the loop expansion corresponds to the chiral expansion.

As an example, at lowest-order the only contributions are those represented by tree-level diagrams with vertices from $\mathcal{L}_2$. One-loop diagrams, $L = 1$, with vertices from $\mathcal{L}_2$ give $D = 4$. Hence in order to calculate one-loop corrections in ChPT, we are required to know the most general NLO effective Lagrangian $\mathcal{L}_4$ and subsequently renormalise its parameters to remove the divergences arising from $\mathcal{L}_2$.

In this work we use the form of $\mathcal{L}_4$ found by Gasser and Leutwyler [66]:

$$\begin{aligned}
\mathcal{L}_4 =& L_1\langle D_\mu U D^\mu U^\dagger\rangle^2 + L_2\langle D_\mu U D_\nu U^\dagger\rangle\langle D^\mu U D^\nu U^\dagger\rangle \\
&+ L_3\langle D_\mu U D^\mu U^\dagger D_\nu U D^\nu U^\dagger\rangle + L_4\langle D_\mu U D^\mu U^\dagger\rangle\langle \chi U^\dagger + U\chi^\dagger\rangle \\
&+ L_5\langle D_\mu U D^\mu U^\dagger(\chi U^\dagger + U\chi^\dagger)\rangle + L_6\langle \chi U^\dagger + U\chi^\dagger\rangle^2 + L_7\langle \chi U^\dagger - U\chi^\dagger\rangle \\
&+ L_8\langle \chi U^\dagger \chi U^\dagger + U\chi^\dagger U\chi^\dagger\rangle + iL_9\langle L_{\mu\nu} D^\mu U D^\nu U^\dagger + R_{\mu\nu} D^\mu U^\dagger D^\nu U\rangle \\
&+ L_{10}\langle L_{\mu\nu} U R^{\mu\nu} U^\dagger\rangle + H_1\langle R_{\mu\nu}R^{\mu\nu} + L_{\mu\nu}L^{\mu\nu}\rangle + H_2\langle \chi^\dagger\chi\rangle.
\end{aligned} \tag{3.92}$$

Introduced here are ten new LECs, L_i, with values that must be determined from phenomenology. The last two terms with coefficients $H_{1,2}$ are only required for the renormalisation of two-point current correlators at one-loop order and since they are independent of the Goldstone boson fields one may conclude that these terms have no phenomenological significance. As previously mentioned, the LECs contain information about the underlying dynamics of full QCD. If one could hypothetically change the masses of the heavy quarks that have been integrated out, the LECs of the effective theory would also change. In principle then, the LECs should be calculable from the full theory. However, doing so

would require us to be able to solve QCD analytically in the non-perturbative regime and therefore, in practice, they are fixed by experimental inputs, theoretical models, and/or LQCD. For the latest LQCD determinations of these LECs one should consult the most recent Flavour Lattice Averaging Group (FLAG) review (see Ref. [69]).

For two-loop diagrams involving only LO vertices the chiral dimension counting expression (Eq. 3.91) tells us the contributions will occur at sixth chiral order. This means additional contributions from the effective chiral Lagrangian up to next-to-next-to-leading-order (NNLO) $\mathcal{O}(q^6)$ are needed to obtain a complete, and physically meaningful, ChPT prediction at NNLO for any physical quantity. The full $\mathcal{O}(q^6)$ SU(3) Lagrangian $\mathcal{L}_6$ in the presence of external sources is given in Ref. [70]. It is found to contain an additional 90 independent LECs plus 4 "contact terms" that are independent of the Goldstone boson fields in the same manner as the constants $H_{1,2}$ appearing in the NLO Lagrangian. This proliferation of coefficients is concerning as it suggests ChPT loses its predictive power unless all the LECs are known at the order one chooses to perform a calculation. Yet not all of the LECs will contribute to any given process. What this means is that in order to make a prediction using ChPT, one only needs to know the specific set of LECs relevant to the process being calculated at the chosen chiral order.

In the next chapter we shall review the calculation of the vector current correlation function in ChPT to two loop order (NNLO). In doing so we shall demonstrate the systematic features of general ChPT analyses that have been introduced here. Recently the $\mathcal{O}(q^8)$ chiral Lagrangian has been determined [71], however calculations of the type we review in the following chapter, while possible in principle, are not yet feasible given the sheer number of terms. We therefore reiterate that the success of ChPT is dependent upon encapsulating the dominant QCD processes at a finite calculable order in the perturbative low-energy expansion, where the contribution from higher orders can be suitably parameterised by an error.

Chapter 4

The Isospin-Breaking Vector Correlator

4.1 Vector Correlation Functions in Chiral Perturbation Theory

The purpose of this section is to review the ChPT calculation of the SIB vector correlation function carried out by Maltman in Ref. [72]. The one-loop $\mathcal{O}(q^2)$ calculation is presented explicitly here to demonstrate the general procedure of loop calculations in ChPT. Aspects of the full two-loop calculation not present in the one-loop analysis, specifically the effects of the renormalised LECs and masses, will also be discussed. The two-loop result shall be quoted; the complete details of the calculation can be found in the main reference given above. Separate analyses of the two-loop vector correlators in ChPT where isospin is conserved at leading order given in Refs. [73, 74] provide additional useful details of the methodology.

The vector correlator, $\Pi^{ab}_{\mu\nu}$ and associated scalar polarisation, Π^{ab}, are defined by

$$\Pi^{ab}_{\mu\nu}(q^2) = (q_\mu q_\nu - q^2 g_{\mu\nu})\Pi^{ab}(q^2) = i\int d^4x e^{iq\cdot x}\langle 0|T\{V^a_\mu(x)V^b_\nu(0)\}|0\rangle. \tag{4.1}$$

where the vector currents, V_μ^a, have the form

$$V_\mu^a = \bar{q}\frac{\lambda^a}{2}\gamma_\mu q \tag{4.2}$$

as described in the ChPT review contained in the previous chapter. The component of the vector correlator relevant to the HVP is the part that describes the vacuum polarisation of the electromagnetic current. This contribution produces the hadronic correction to the propagator of the internal photon in Fig. 2.1 represented by the shaded circle in Fig. 3.1. The photon couples to both isoscalars (I=0) and isovectors (I=1) and the three-flavor, light u,d, and s quark contribution to the electromagnetic current is given by

$$J_\mu^{EM} = V_\mu^3 + \frac{1}{\sqrt{3}}V_\mu^8. \tag{4.3}$$

Hence the propagator for the EM current, $\langle 0|T\{J_\mu^{EM}J_\nu^{EM}\}|0\rangle$, can be decomposed into four pieces: two with $a = b = 3, 8$ which we refer to as 33, 88, and also two with $a \neq b$ referred to as 38 and 83. This notation is consistent with Refs. [72, 74].

There is no leading-order, $\mathcal{O}(m_u - m_d)$, SIB contribution to either of the 33 or 88 pieces as can be made clear by the following argument. Given that the vacuum has isospin I=0, vacuum matrix elements are only non-zero for operators (or products of operators) that also have I=0. Note that the *u*-*d* mass-difference operator, presented in Eq. 3.77, has $I = 1$ and hence a non-vanishing $\mathcal{O}(m_u - m_d)$ contribution to the vacuum matrix element of a product of two currents will occur only if the product of the two currents with the mass-difference operator has an I=0 component. This scenario is only possible if the product of the two currents itself has an I=1 component. In the 88 case, this is impossible since the product of two I=0 currents necessarily also has I=0. The reasoning is slightly more complicated for the 33 case, involving the product of two I=1 currents. An I=1 object is represented by a 3-vector, and the I=1 combination of two such I=1 objects is given by their cross product. This cross product vanishes in the case where the two vectors being

combined are the same, and for this reason we find that the product of the two identical I=1 currents appearing in Π^{33} also has no I=1 component. In contrast, the product of the I=1 and I=0 components of the EM current necessarily has I=1, and will therefore combine with the I=1 $\mathcal{O}(m_d - m_u)$ SIB mass-difference operator to produce a non-zero $\mathcal{O}(m_d - m_u)$ SIB contribution to Π^{38}.

The $a = b = 3, 8$ parts of the polarisation function were calculated to two loops by Amorós, Bijnens and Talavera [73]. Since in this work we are focused solely on the leading-order SIB correction to the muon $g - 2$, the result of the 38 analysis in Ref. [72] provides all we need from ChPT at two-loop order to predict the effect. Both $a \neq b$ pieces, 38 and 83, are equivalent to each other and hence the leading-order SIB component of the vector correlator can be obtained through just the 38 correlator. SIB effects are generated by the $a = b$ correlators, but these effects can be neglected since they enter beginning only at $\mathcal{O}(m_u - m_d)^2$.

4.2 The One-Loop Calculation of the Vector Correlator $\Pi^{38}_{\mu\nu}$

The one-loop diagrams that are required to be evaluated for the $\mathcal{O}(q^4)$ vector correlator calculation are given in Fig. 4.1. The general procedure of calculating loop diagrams for the vector correlators in ChPT is to expand the Lagrangian to the required order in the fields, then take functional derivatives with respect to the external vector sources $v_\mu \equiv v^a_\mu \lambda_a/2$. The loop integrals can then be evaluated and the counterterms determined using the $\overline{\text{MS}}$ renormalisation scheme (described in most contemporary QFT textbooks, see Ref. [43]). The loop calculations yield standard quantities in QFT perturbation theory which are covered in detail in Ref. [75].

We begin with the leading-order effective chiral Lagrangian, Eq. 3.90,

$$\mathcal{L}_2 = \frac{f^2}{4}\langle D_\mu U D^\mu U^\dagger \rangle + \frac{f^2}{2} B_0 \langle \mathcal{M}(U^\dagger + U) \rangle. \tag{4.4}$$

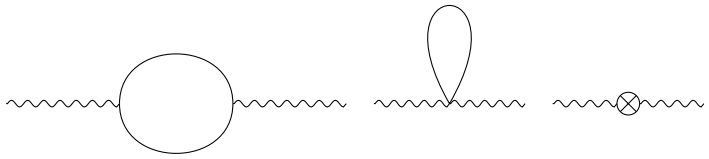

Figure 4.1: The one-loop graphs for $\Pi^{\mu\nu}$. A single external vector source represented by the incoming line to the left of each graph undergoes a transition to an outgoing external vector source. The internal lines are pseudoscalar meson propagators, π, K, η. Lastly, the crossed circle represents the $\mathcal{O}(q^4)$ vertex insertion.

For the tadpole diagram, the middle diagram of Fig. 4.1, we are solely interested in terms with two Goldstone fields coupled to two vector sources. Expanding the covariant derivatives we find

$$\mathcal{L}_2^{tad} = \frac{f^2}{4}\mathrm{Tr}(-v_\mu U v^\mu U^\dagger - U v_\mu U^\dagger v^\mu). \tag{4.5}$$

Now we perform an expansion of U, keeping only terms second order in ϕ

$$\begin{aligned}\mathcal{L}_2^{tad} &= -\frac{f^2}{4}\mathrm{Tr}\left[\frac{1}{2}v_\mu v^\mu\big(\frac{-i\phi}{f}\big)^2 + \frac{1}{2}v_\mu\big(\frac{i\phi}{f}\big)^2 v^\mu + v_\mu\frac{\phi}{F_0}v^\mu\frac{\phi}{f} + \frac{1}{2}\big(\frac{i\phi}{f}\big)^2 v_\mu v^\mu + \frac{1}{2}v_\mu\big(\frac{-i\phi}{F_0}\big)^2 v^\mu + \frac{\phi}{f}v_\mu\frac{\phi}{f}v^\mu\right] \\ &= \frac{1}{2}\mathrm{Tr}\left[\phi^2 v^\mu v_\mu - \phi v^\mu \phi v_\mu\right]\end{aligned} \tag{4.6}$$

where the cyclic property of the trace was used repeatedly. Next we can evaluate the trace by expressing the fields in index form,

$$\begin{aligned}\mathcal{L}_2^{tad} &= \frac{1}{2}\mathrm{Tr}\left[\lambda_c\phi_c\lambda_d\phi_d\frac{1}{2}\lambda_a v_a^\mu\frac{1}{2}\lambda_b v_{b,\mu} - \lambda_c\pi_c\frac{1}{2}\lambda_a v_a^\mu\lambda_d\phi_d\frac{1}{2}\lambda_b v_{b,\mu}\right] \\ &= \frac{1}{8}\phi_c\phi_d v_a^\mu v_{b,\mu}\mathrm{Tr}\left[\lambda_c\lambda_d\lambda_a\lambda_b - \lambda_c\lambda_a\lambda_d\lambda_b\right] \\ &= \frac{1}{8}\phi_c\phi_d v_a^\mu v_{b,\mu}\mathrm{Tr}\left[\lambda_d\lambda_a[\lambda_b,\lambda_c]\right].\end{aligned} \tag{4.7}$$

The commutator can be evaluated using the SU(3) Lie algebra,

$$\begin{aligned}\mathcal{L}_2^{tad} &= \frac{1}{8}\phi_c\phi_d v_a^\mu v_{b,\mu}\mathrm{Tr}\Big[\lambda_d\lambda_a(2if_{bcg}\lambda_g)\Big] \\ &= \frac{i}{4}f_{bcg}\phi_c\phi_d v_a^\mu v_{b,\mu}\mathrm{Tr}\Big[\lambda_d\lambda_a\lambda_g\Big] \\ &= \frac{i}{4}f_{bcg}\phi_c\phi_d v_a^\mu v_{b,\mu}(2if_{dag}) \\ &= \frac{1}{2}f_{adg}f_{bcg}\phi_c\phi_d v_a^\mu v_{b,\mu} \end{aligned} \tag{4.8}$$

where the fine structure constants f_{abc} are totally antisymmetric in the three indices, analogous to the Levi-Civita symbol in SU(2).

$$f_{abc} = \begin{cases} 1, & abc = 123, +\text{cyclic permutations} \\ \frac{1}{2}, & abc = 147,\ 165,\ 257,\ 345,\ 376, +\text{c.p.} \\ \frac{\sqrt{3}}{2}, & abc = 458,\ 678, +\text{c.p.} \\ 0, & \text{otherwise.} \end{cases} \tag{4.9}$$

For the unitarity diagram, this process is repeated keeping only the terms with two Goldstone fields coupled to one vector source. The full interaction Lagrangian needed for the one loop calculations is given by,

$$\mathcal{L}_2^{int} = -f_{abc}\phi_b\partial_\mu\phi_c v_a^\mu + \frac{1}{2}f_{adg}f_{bcg}\phi_c\phi_d v_a^\mu v_b^\nu. \tag{4.10}$$

First we find the vertex factor. For $a = 3, b = 8$ the two fine structure constants in the term,

$$\frac{1}{2}f_{3dg}f_{8cg}\phi_c\phi_d v_3^\mu v_8^\nu, \tag{4.11}$$

can only give factors of $\pm\sqrt{3}/4$. Expanding out this term, we can write the interaction in

terms of the physical fields via

$$\begin{aligned}\frac{1}{2}f_{3dg}f_{8cg}\phi_c\phi_d v_3^\mu v_8^\nu &= \frac{\sqrt{3}}{8}(\phi_4\phi_4+\phi_5\phi_5-\phi_6\phi_6-\phi_7\phi_7)v_3^\mu v_8^\nu \\ &= \frac{\sqrt{3}}{4}(K^-K^+-\bar{K}^0K^0)v_3^\mu v_8^\nu \end{aligned} \tag{4.12}$$

which therefore gives rise to vertex factors of

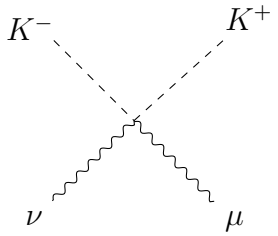

$$= \frac{\sqrt{3}}{2}ig^{\mu\nu}, \tag{4.13}$$

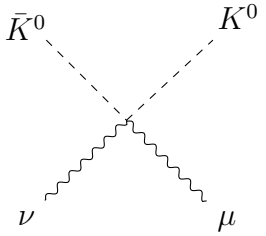

$$= -\frac{\sqrt{3}}{2}ig^{\mu\nu}, \tag{4.14}$$

where an additional factor of 2 in the numerator is a symmetry factor. The tadpole contribution is then found by multiplying the vertex factors by integrals over the momenta of the internal propagators,

$$\mathcal{M}_{38}^{\mu\nu}\Big|_{tad} = i\frac{\sqrt{3}}{2}\big[A(m_{K^+}^2)-A(m_{K^0}^2)\big]g^{\mu\nu}, \tag{4.15}$$

where the loop integral

$$A(m^2) = \int \frac{d^dq}{(2\pi)^d}\frac{1}{q^2-m^2} \tag{4.16}$$

is evaluated using the standard method of dimensional regularisation[1]. In the isospin limit, $m_d = m_u$, the charged and neutral kaon masses are the same and cause the tadpole amplitude to vanish. Similarly for the unitarity graphs, the amplitude vanishes in the equal

[1]Dimensional regularisation was introduced by 't Hooft and Veltman in Ref. [76] and is covered in most standard introductory QFT texts, see Chapter 7 of Ref. [43].

mass limit, which we can show by first considering the vertices that arise from the term

$$-f_{abc}\phi_b\partial_\mu\phi_c v_a^\mu$$

which in momentum space introduces a factor of momentum of the Goldstone fields, $\partial_\mu \to iq_\mu$.

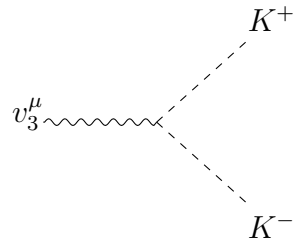

$$= -\frac{i}{2}(q+q')^\mu \tag{4.17}$$

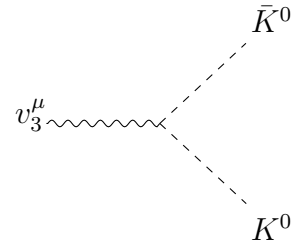

$$= -\frac{i}{2}(q+q')^\mu \tag{4.18}$$

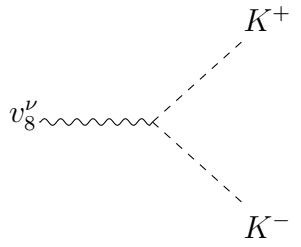

$$= -\frac{i\sqrt{3}}{2}(q+q')^\nu \tag{4.19}$$

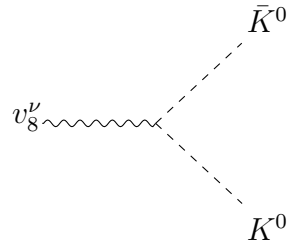

$$= -\frac{i\sqrt{3}}{2}(q+q')^\nu \tag{4.20}$$

where q and q' label the incoming and outgoing loop momenta respectively. The unitarity

amplitude is then given by,

$$\begin{aligned}\mathcal{M}_{38}^{\mu\nu}\Big|_{uni} &= -\frac{i\sqrt{3}}{4}\Bigg[\int\frac{d^dq}{(2\pi)^d}\frac{(2q-k)^\mu}{q^2-m_{K^+}^2}\frac{(2q-k)^\nu}{(q-k)^2-m_{K^+}^2} \\ &\quad -\int\frac{d^dq}{(2\pi)^d}\frac{(2q-k)^\mu}{q^2-m_{K^0}^2}\frac{(2q-k)^\nu}{(q-k)^2-m_{K^0}^2}\Bigg] \\ &= -\frac{i\sqrt{3}}{4}\left[T^{\mu\nu}(m_{K^+}^2)-T^{\mu\nu}(m_{K^0}^2)\right] \end{aligned} \tag{4.21}$$

where dimensional regularisation has again been used and, in the regularisation method, $T^{\mu\nu}$ consists of four quantities

$$\begin{aligned} T^{\mu\nu} &= 4B^{\mu\nu}+q^\mu q^\nu B-2q^\mu B^\nu-2q^\nu B^\mu \\ &= 2A(m^2)g^{\mu\nu}+(q^\mu q^\nu-q^2g^{\mu\nu})\left(\frac{A(m^2)}{3m^2}+4\bar{B}_{21}(q^2,m^2)\right) \end{aligned} \tag{4.22}$$

where the expressions for $B^{\mu\nu}, B^\mu, B$ are

$$\{B,B_\mu,B_{\mu\nu}\}\equiv\int\frac{d^dk}{(2\pi)^d)}\frac{\{1,k_\mu,k_\mu k_\nu\}}{[k^2-m^2][(k-q)^2-m^2]} \tag{4.23}$$

and $\bar{B}_{21}$ is

$$\bar{B}_{21}(m^2,q^2)=\frac{1}{12}\left(1-\frac{4m^2}{q^2}\right)\bar{B}(m^2,q^2)-\frac{i}{576\pi^2} \tag{4.24}$$

where $\bar{B}$ is the subtracted function

$$\bar{B}(m^2,q^2)=B(m^2,q^2)-B(m^2,0). \tag{4.25}$$

There are no contributions to the 38 correlator from the counterterm diagram on the right hand side of Fig. 4.1. Such a diagram would be generated by terms in $\mathcal{L}_4$ that contain two external vector sources only. The only terms where this configuration is possible are those with coefficients L_{10} and H_1 in $\mathcal{L}_4$ which contain, for our purposes where we consider

external vector sources only, the vector field strength tensors,

$$F_{\mu\nu} = \partial_\mu v_\nu - \partial_\nu v_\mu - i[v_\mu, v_\nu]. \tag{4.26}$$

The quark mass matrix $\mathcal{M}$ does not appear at all in these terms and it is therefore evident that there is no $\mathcal{L}_4$ LEC contribution to the leading-order IB 38 correlator which we know must consist of terms proportional to the quark mass difference $(m_d - m_u)$ at leading-order. Hence the full 38 vector correlator at next-to-leading order is found to be the sum of the expressions in Eqns. 4.15 and 4.21,

$$\Pi^{38}_{\mu\nu}(q^2) = i\frac{\sqrt{3}}{4}(q_\mu q_\nu - q^2 g^{\mu\nu})(T_1(K^0) - T_1(K^+)), \tag{4.27}$$

where

$$T_1(m^2, q^2) = \left[4\bar{B}_{21}(m^2, q^2) + \frac{A(m^2)}{m^2} + \mathcal{O}(d-4)\right] \tag{4.28}$$

It is noted that this result is finite and independent of the renormalisation scale, μ. These facts are pointed out in Ref. [72] and are straightforward to see from the expressions.

The 38 correlator to two-loops $\mathcal{O}(q^6)$

The result of the complete two-loop calculation for the scalar correlator, $\Pi^{38}_{\mu\nu} = (q_\mu q_\nu - q^2 g_{\mu\nu})\Pi^{38}$ is given by equation 3.19 of Ref. [72],

$$\begin{aligned}\Pi^{38}(q^2) =& \frac{\sqrt{3}}{4}(M^2_{K^0} - M^2_{K^+})_{QCD}\Bigg[- \frac{2i\bar{B}(\bar{M}^2_K, q^2)}{q^2} \\ &\times \left(1 + \frac{2q^2}{f^2}\left[2L^r_9 - i(\bar{B}_{21}(M^2_\pi, q^2) + \bar{B}_{21}(\bar{M}^2_K, q^2) - \frac{1}{192\pi^2}\log\frac{M^2_\pi \bar{M}^4_K}{\mu^6}\right]\right) \\ &- \frac{L^r_9 + L^r_{10}}{2\pi^2 f^2}\left(1 + \log\frac{\bar{M}^2_K}{\mu^2}\right) + \frac{16}{3f^2}\hat{Q}^r\Bigg].\end{aligned} \tag{4.29}$$

where $(M^2_{K^0} - M^2_{K^+})_{QCD}$ is the non-EM contribution to the kaon mass-squared splitting, $\bar{M}^2_K$ is the average of the non-EM portion of the physical neutral, K^0 and charged, K^+,

kaon masses-squared, L_9^r and L_{10}^r are low energy constant from the next-to-leading order chiral Lagrangian, $\mathcal{L}_4$, $\hat{Q}^r$ is the tree-level LEC at $\mathcal{O}(q^6)$, and μ is the mass scale in the $\overline{\text{MS}}$ renormalisation scheme. Typically in ChPT a scale corresponding to the light resonances is used since these are degrees of freedom that were integrated out with the rest of the heavy fields in the formulation of the chiral Lagrangian.

An important feature of this expression concerns the squared masses appearing inside the loop integral functions. As discussed in the original paper, the masses which appear in the $\mathcal{O}(q^4)$ expression can be recast as the difference between the radiatively-corrected (one-loop) masses, $M_{K^+,0}^2$, and the $\mathcal{O}(q^4)$ corrections, $\Delta_{K^+,0}$

$$m_{K^+,0}^2 = M_{K^+,0}^2 + \Delta_{K^+,0}. \tag{4.30}$$

In the two-loop amplitudes, the lowest order expressions for the meson masses can be set to $M_{K^+,0}^2$ since the error occurs at higher order. For the one-loop amplitudes, this substitution leads to cancellation with terms generated by the tree-level $\mathcal{O}(q^6)$ diagram and a simplification of the overall expression. This is also discussed in the context of the 33 and 88 correlators in Ref. [74]. Afterwards $M_{K^+,0}^2$ are set to the physical kaon masses.

Another salient feature of the expression presented here is the presence of the renormalised counterterms, L_{10}^r and L_9^r from $\mathcal{L}_4$, and the $\mathcal{O}(q^6)$ LEC $\hat{Q}^r$, which is proportional to what is referred to in the contemporary literature as C_{61} (see Refs. [77,78]). The $\mathcal{O}(q^6)$ LEC is seen to generate significant corrections to the 38 correlator, raising the possibility that the chiral series for the correlator may not be well-converged at NNLO. This is an aspect of the chiral prediction which can be investigated through application to the muon $g-2$. By comparing the ChPT prediction of the leading-order SIB contribution to the muon $g-2$, obtained from this correlator by a process that will be detailed in a subsequent chapter, one can analyse the extent to which the NNLO ChPT prediction captures the dominant low-energy hadronic physics and therefore make predictions about the size of corrections from higher order in the chiral expansion.

Chapter 5

Results

5.1 Formulation of the Leading-Order Hadronic Vacuum Polarisation Contribution to the Muon $g-2$

The leading order, $\mathcal{O}(\alpha^2)$, hadronic vacuum polarisation (LO-HVP) contribution to the anomalous magnetic moment of the muon, $a_\mu = (g-2)/2$, is given in the Euclidean momentum-squared, Q^2, formulation by a weighted integral of the subtracted photon vacuum polarisation function, $\hat{\Pi}(Q^2) = \Pi(Q^2) - \Pi(0)$. The expression, which represents the contribution shown in Fig. 3.1 is

$$a_\mu^{LO-HVP} = -4\alpha^2 \int_0^\infty dQ^2 f(Q^2)\hat{\Pi}(Q^2) \tag{5.1}$$

where α is the electromagnetic fine structure constant, and $f(Q^2)$ is an exactly known kernel which diverges as $1/\sqrt{Q^2}$ as $Q^2 \to 0$. Explicitly,

$$f(Q^2) = \frac{m_\mu^2 Q^2 Z^3 (1 - Q^2 Z)}{1 + m_\mu^2 Q^2 Z^2} \tag{5.2}$$

where

$$Z = -\left[\frac{Q^2 - (Q^4 + 4m_\mu^2 Q^2)^{1/2}}{2m_\mu^2 Q^2}\right]. \tag{5.3}$$

As discussed in the previous chapter, the HVP is evaluated by calculating the correlation function of the product of vector currents, $\langle 0|J_\mu^{EM} J_\nu^{EM}|0\rangle$. This product is composed of pieces denoted 33, 88, 38 and 83, where the labels 3 and 8 specify the I=1 and I=0 parts of the EM current respectively. In the previous chapter the 33 and 88 parts of the EM correlator were shown to receive no $\mathcal{O}(m_u - m_d)$ SIB contributions, so the leading order, $\mathcal{O}(m_u - m_d)$, SIB contributions are due entirely to the the 38 and 83 pieces, which are identical, and equal to $\langle 0|V_\mu^3 V_\nu^8|0\rangle$. We justify ignoring terms that are higher order in $m_d - m_u$ by assuming the u-d quark mass difference is small and thus that higher order SIB contributions may be safely neglected. The resulting (leading-order) SIB component of the photon vacuum polarisation is then

$$\Pi^{SIB}(q^2) = \frac{2}{\sqrt{3}}\Pi^{38}(q^2) \tag{5.4}$$

where the factor of 2 comes from adding together the equivalent 38 and 83 scalar correlators and the $1/\sqrt{3}$ comes from the vector current composition of the electromagnetic current given by Eq. 4.3.

The first step towards finding the SIB contribution to the LO-HVP component of a_μ is to take the two-loop expression for the polarisation function $\Pi^{38}(q^2)$ from Ref. [72] and rewrite it in terms of the Euclidean momentum-squared, $Q^2 = -q^2$. The result is

$$\begin{aligned}\Pi^{38}(Q^2) =& \frac{\sqrt{3}}{4}(M_{K^0}^2 - M_{K^+}^2)_{QCD}\Bigg[\frac{2i\bar{B}(\bar{M}_K^2, Q^2)}{Q^2}\Bigg(1- \\ & \frac{2Q^2}{f^2}\big[2L_9^r(\mu) - i(\bar{B}_{21}(M_\pi^2, Q^2) + 2\bar{B}_{21}(\bar{M}_K^2, Q^2) - \frac{1}{192\pi^2}\log\frac{M_\pi^2\bar{M}_K^4}{\mu^6}\big]\Bigg) \\ & - \frac{L_9^r(\mu) + L_{10}^r(\mu)}{2\pi^2 f^2}\left(1 + \log\frac{\bar{M}_K^2}{\mu^2}\right) + \frac{16}{3f^2}\hat{Q}^r(\mu)\Bigg].\end{aligned} \tag{5.5}$$

This polarisation function is independent of μ, as it should be, provided the values used for the scale-dependent LECs $L_9^r(\mu)$ and $L_{10}^r(\mu)$ are those corresponding to the μ used in the log terms in this expression. In this work, we perform our analysis using the scale $\mu = m_\rho = 770$ MeV. The definition of the auxiliary functions $\bar{B}_{21}(M^2, Q^2)$ presented in

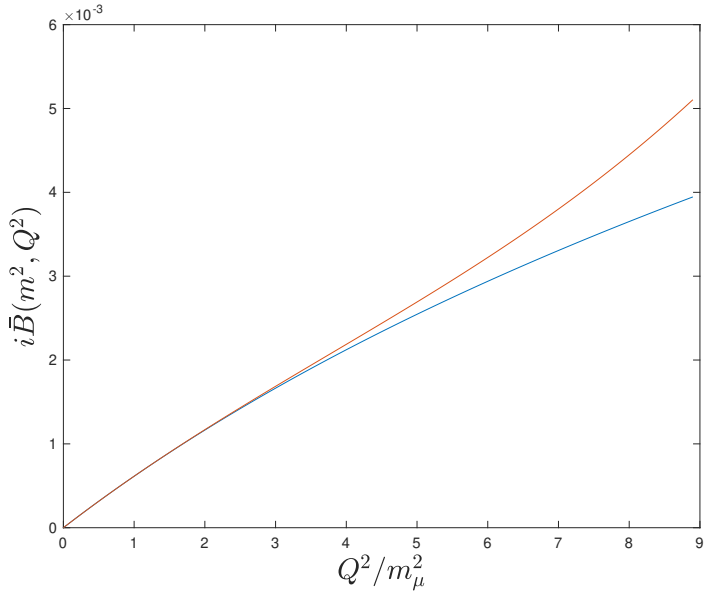

Figure 5.1: The loop integral function $i\bar{B}$ plotted in units of Q^2/m_μ^2. The blue line shows the exact form whereas the red line plots the low-Q^2 approximation given by Eq. 5.9.

the previous chapter contains the subtracted loop integral function

$$\bar{B}(M^2, Q^2) = -\frac{i}{16\pi^2}\int_0^1 \log\left(1 + Q^2 x(1-x)/M^2\right) \tag{5.6}$$

which also appears explicitly in Eq. 5.5 and has an explicit analytical form in the region $Q^2 > 0$ given by

$$\bar{B}(M^2, Q^2) = \frac{i}{8\pi^2}\left[1 - \sqrt{1 + 4M^2/Q^2}\,\tanh^{-1}\left(\frac{1}{\sqrt{1 + 4M^2/Q^2}}\right)\right]. \tag{5.7}$$

The Euclidean momentum-squared formulation of a_μ^{HVP} requires the SIB polarisation to be written in the subtracted form,

$$\hat{\Pi}^{SIB}(Q^2) = \Pi^{SIB}(Q^2) - \Pi^{SIB}(0), \tag{5.8}$$

and therefore one must determine an expression for $\Pi^{38}(0)$. This can be accomplished using the fact that the loop integral function $\bar{B}(M^2, Q^2)$ can be written as an expansion

in powers of Q^2/M^2,

$$\bar{B}(M^2,Q^2) = -\frac{i}{96\pi^2}\frac{Q^2}{M^2} + \frac{i}{960\pi^2}\frac{Q^4}{M^4} - \frac{i}{6720\pi^2}\frac{Q^6}{M^6} + ... \tag{5.9}$$

where Fig. 5.1 shows a comparison of the original function and the low-energy expansion. From this expression one finds that the corrections which appear on the second and third lines of Eq. 5.5 vanish in the $Q^2 \to 0$ limit. Applying the same method of expanding about the $Q^2 = 0$ limit of the remaining $\bar{B}(\bar{M}_K^2, Q^2)$ in the first line of Eq. 5.5 we find that the polarisation function reduces to a constant term given by

$$\Pi^{38}(0) = \frac{\sqrt{3}}{4}(M_{K^0}^2 - M_{K^+}^2)_{QCD}\left[\frac{1}{48\pi^2\bar{M}_K^2}\right]. \tag{5.10}$$

The subtracted 38 polarisation function at two loops, found by subtracting this constant from the expression for $\Pi^{38}(Q^2)$ is given by

$$\begin{aligned}\hat{\Pi}^{38}(Q^2) =& \frac{\sqrt{3}}{4}(M_{K^0}^2 - M_{K^+}^2)_{QCD}\times \\ & \left[-\frac{1}{48\pi^2\bar{M}_K^2} + \frac{2i\bar{B}(\bar{M}_K^2,Q^2)}{Q^2}\left\{1 - \right.\right. \\ & \left.\left. \frac{2Q^2}{f^2}\left(2L_9^r(\mu) - i(\bar{B}_{21}(M_\pi^2,Q^2) + 2\bar{B}_{21}(\bar{M}_K^2,Q^2)) - \frac{1}{192\pi^2}\log\frac{M_\pi^2\bar{M}_K^4}{\mu^6}\right)\right\}\right].\end{aligned} \tag{5.11}$$

which vanishes, by construction, at $Q^2 = 0$. One additionally finds that the subtracted polarisation function diverges logarithmically as $Q^2 \to \infty$.

SIB appears in this expression through the QCD mass-squared splitting of the neutral and charged kaons which is proportional to $m_d - m_u$ at leading order in ChPT. The isolation of the leading order SIB component of the photon vacuum polarisation at Euclidean Q^2 leads us directly to an expression for the leading order SIB contribution to the value of a_μ,

$$a_\mu^{SIB} = -4\alpha^2\int_0^\infty dQ^2 f(Q^2)\hat{\Pi}^{SIB}(Q^2) \tag{5.12}$$

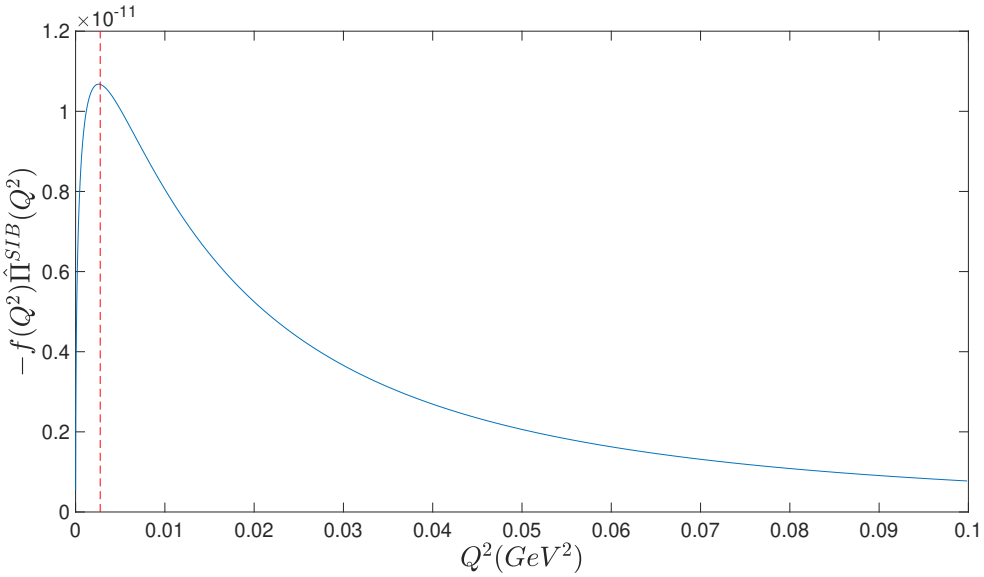

Figure 5.2: The integrand of Eq. 5.12 shown for values of Q^2 up to 0.1 GeV^2. The dashed vertical line is a marker at the position $Q^2 \sim (m_\mu/2)^2$, showing that the peak is in the typical position set by the mass of the muon.

where $\hat{\Pi}^{SIB}(Q^2)$ is the subtracted Euclidean form of Eq. 5.4,

$$\hat{\Pi}^{SIB}(Q^2) = \frac{2}{\sqrt{3}}\hat{\Pi}^{38}(Q^2) \tag{5.13}$$

A plot showing the behaviour of the resulting integrand in Eq. 5.12 is given in Fig. 5.2.

5.2 Numerical Method

A Romberg integration routine based upon successive iterations of the trapezoidal rule is used to evaluate a_μ^{SIB}. ChPT is only valid in the low-Q^2 regime and it is therefore unreasonable to trust results obtained by integrating to arbitrarily high values of Q^2. Hence we are required to cut off the integration at some upper limit Q^2_{max} reflecting our confidence in the validity of the ChPT prediction. The method employed here is to carry out the integration over a range of values for Q^2_{max} up to $m_\eta^2 \sim 0.3$ GeV^2 since the η meson has the largest mass of the degrees of freedom retained by the SU(3) effective chiral Lagrangian after the heavy fields were integrated out. Therefore we expect ChPT to

produce sensible results at momentum scales corresponding to, but not greater than, m_η. In comparison, we would not expect results from an analysis using integration cutoff at the scale of the lightest resonances, $m_\rho^2 \simeq 0.6$ GeV^2, to be reliable.

The integration is possible the entire way down to $Q^2 = 0$ despite the divergence of the electromagnetic kernel, $f(Q^2)$. To see this, one may take the limit of the functions within both the kernel and the polarisation function as $Q^2 \to 0$, keeping only the leading order terms.

$$\lim_{Q^2\to 0} Z = \frac{1}{m_\mu\sqrt{Q^2}} - \frac{1}{2m_\mu^2} + \mathcal{O}(\sqrt{Q^2}) \tag{5.14}$$

$$\approx \frac{1}{m_\mu\sqrt{Q^2}}. \tag{5.15}$$

$$\lim_{Q^2\to 0} f(Q^2) = \frac{1}{2m_\mu\sqrt{Q^2}} - \frac{1}{2m_\mu^2} + \mathcal{O}(\sqrt{Q^2}) \tag{5.16}$$

$$\approx \frac{1}{2m_\mu\sqrt{Q^2}} \quad \text{for } \sqrt{Q^2} \ll m_\mu. \tag{5.17}$$

In doing so one finds that to leading order in Q^2 the expression for the full integrand is given by

$$\begin{aligned} -4\alpha^2 f(Q^2)\hat{\Pi}^{SIB}(Q^2) = &-\frac{\alpha^2}{m_\mu}(M_{K^0}^2 - M_{K^+}^2)_{QCD}\bigg[-\frac{1}{480\pi^2}\frac{\sqrt{Q^2}}{\bar{M}_K^4} \\ &-\frac{1}{24\pi^2 f^2}\frac{\sqrt{Q^2}}{\bar{M}_K^2}\left(2L_9^r - \frac{1}{64\pi^2} - \frac{1}{192\pi^2}\log\frac{M_\pi^2\bar{M}_K^4}{\mu^6}\right)\bigg] + \mathcal{O}((Q^2)^{3/2}). \end{aligned} \tag{5.18}$$

It is clear from this expression that the integrand vanishes in the $Q^2 \to 0$ limit. The integrand written in this form is used to handle the divergence of $f(Q^2)$ in the numerical method by using it in place of the full expression at suitably small values of Q^2.

5.3 Input Parameters and the SIB Contribution to the Kaon Mass Splitting

In this work we use the following values for the low energy constants (LECs) of ChPT appearing in our expression:

$$L_9^r(770) = 5.93(43) \times 10^{-3}, \tag{5.19}$$

from Ref. [79], and

$$f = 80.3(2.5)(5.4) \text{ MeV} \tag{5.20}$$

from Ref. [80].

In order to obtain the numerical input value of the QCD mass-squared splitting of the kaons we need to subtract the electromagnetic contribution. In the SU(3) chiral limit this can be done using Dashen's theorem, an SU(3) chiral limit result which states that

$$(M_{\pi^+}^2 - M_{\pi^0}^2)_{EM} = (M_{K^+}^2 - M_{K^0}^2)_{EM}. \tag{5.21}$$

This relation receives corrections away from the chiral limit, which are conventionally parameterised by a constant, ϵ, defined by

$$\epsilon = \frac{(M_{K^+}^2 - M_{K^0}^2)_{EM} - (M_{\pi^+}^2 - M_{\pi^0}^2)_{EM}}{(M_{\pi^+}^2 - M_{\pi^0}^2)}. \tag{5.22}$$

Since the mass-squared splitting of the pions does not receive $\mathcal{O}(m_d - m_u)$ corrections we can use $(M_{\pi^+}^2 - M_{\pi^0}^2)_{EM} = (M_{\pi^+}^2 - M_{\pi^0}^2)$ to rewrite this expression to leading order in isospin breaking as

$$\epsilon = \frac{(M_{K^+}^2 - M_{K^0}^2)_{EM}}{(M_{\pi^+}^2 - M_{\pi^0}^2)} - 1. \tag{5.23}$$

The kaon mass-squared splitting in QCD can be written as the difference of the kaon

physical and electromagnetic mass-squared splittings,

$$(M^2_{K^0} - M^2_{K^+})_{QCD} = (M^2_{K^0} - M^2_{K^+}) - (M^2_{K^0} - M^2_{K^+})_{EM}. \tag{5.24}$$

By substituting Eq. 5.23 into this expression, the QCD kaon mass-squared splitting can be rewritten in the form

$$(M^2_{K^0} - M^2_{K^+})_{QCD} = (M^2_{K^0} - M^2_{K^+}) - (1+\epsilon)(M^2_{\pi^0} - M^2_{\pi^+}) \tag{5.25}$$

and hence the value used in our analysis is found directly from the observed pion and kaon masses, and the Dashen's theorem violation parameter ϵ.

From the 2019 FLAG review [69], the value of ϵ is determined, in the renormalisation scheme chosen there to define the separation of the strong and EM isospin-breaking contributions, to be

$$\epsilon = 0.79(7). \tag{5.26}$$

For the remaining masses appearing in Eq. 5.11 we have used the values given in Ref. [81], using that same convention

$$\bar{M}_K = 494.2(5)\ \text{MeV}, \qquad M_\pi = 134.8(3)\ \text{MeV}. \tag{5.27}$$

5.4 NNLO Prediction: Results and Discussion

From our calculations we find a leading-order SIB contribution to the muon's anomalous magnetic moment at NNLO in the chiral expansion of

$$a_\mu^{SIB}\Big|_{\text{NNLO}} = 0.82(12) \times 10^{-10}. \tag{5.28}$$

where the error is determined by the adding in quadrature the 1σ contributions to the value of a_μ^{SIB} of f, L_9^r and ϵ. Estimations from the ratio of the $u-d$ mass difference to the QCD scale predict the size of SIB effects to be at $(m_d - m_u)/\Lambda_{QCD} \sim 1\%$ of the total hadronic contribution. Taking the result of the current best dispersive analysis determination of the LO-HVP [55], since this quantity dominates the hadronic contribution, one expects SIB effects at the $\sim 7 \times 10^{-10}$ level. However, the NNLO ChPT result predicts the scale of SIB effects to be at the 0.1% level.

The most precise determination of the SIB contribution to a_μ from LQCD to date is the 2019 result published by the ETM collaboration [9]. In that study, employing the same strong-EM separation scheme employed by FLAG, the SIB contribution was found to be

$$\left[a_\mu^{SIB}\right]_{\text{ETM}} = 6.0(2.3) \times 10^{-10} \tag{5.29}$$

which matches the order of the phenomenological prediction and is consistent with the results of two earlier, less precise lattice determinations, $a_\mu^{SIB} = 10.6(8.0) \times 10^{-10}$ from the RBC/UKQCD collaboration [10, 11] and $9.0(4.5) \times 10^{-10}$ from the Fermilab Lattice, HPQCD, and MILC Collaborations [12].

The NNLO ChPT prediction is small, at just 14% of the ETM determination, and therefore further analysis is required in order to understand the cause of the discrepancy found in comparison with the Lattice results. One can immediately rule out the systematic integration cutoff used in the numerical analysis of Eq. 5.12. At $Q^2_{max} = m_\eta^2$ we are already at the upper limit of confidence in the predictive ability of SU(3) ChPT. Furthermore, if one were to increase the cutoff, for example, to the scale of the ρ resonance, well beyond the domain of validity of ChPT, the NNLO prediction would still remain far below the level required for consistency with the ETM determination. This comprehensively rules out the possibility that a plausible higher integration cutoff scale exists that would produce a result which resolves this discrepancy.

Critiquing the extent to which our NNLO ChPT prediction encapsulates the bulk of

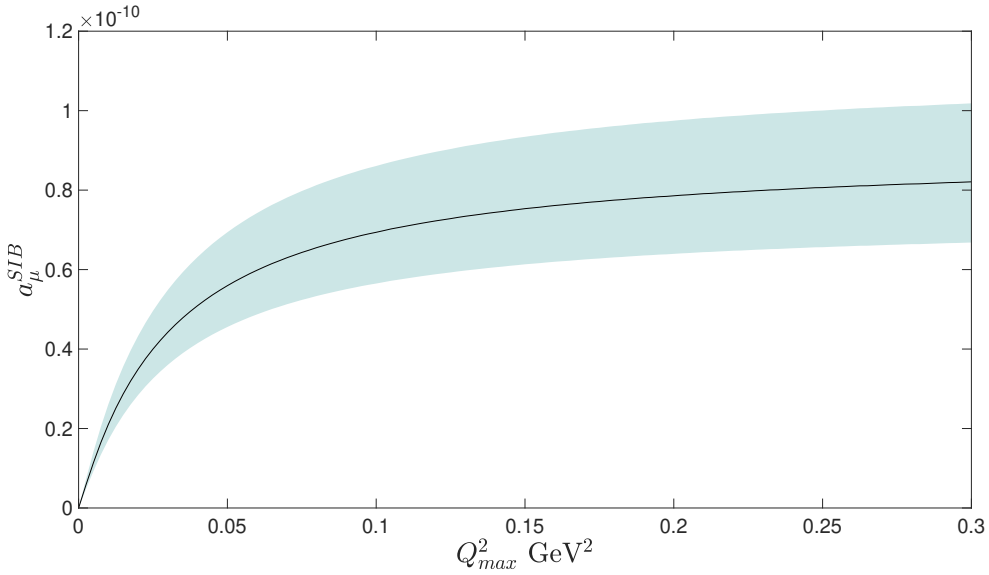

Figure 5.3: NNLO ChPT results for a_μ^{SIB} as a function of the integration cutoff Q^2_{max} up to m_η^2. The error band is generating by repeating the analysis and allowing the quantities associated with the most significant uncertainties (f, L_9^r, ϵ) to vary within their $\pm 1\sigma$ error ranges.

the relevant physical processes in the SIB contribution, there is good evidence to support the conclusion that our NNLO expression in Eq. 5.11 has important shortcomings. If one studies Maltman's expression for $\Pi^{38}(q^2)$ in Eq. 4.29 then it can be seen that the NNLO contribution is larger than the NLO one. Furthermore, given the increase in size between the NLO and NNLO contributions, there remains the potential for even higher order contributions to be significant relative to those already calculated. While an order-by-order size comparison is at this stage insufficient justification of a convergence argument, one should immediately note the absence of the NNLO LEC referred to as $\hat{Q}^r$ in Maltman's calculation (proportional to C_{61} in the contemporary convention) in the subtracted expression given here by Eq. 5.11. The term involving this constant in the unsubtracted expression represents the major contribution to the overall size of the vacuum polarisation. The absence of this contribution in the NNLO ChPT representation of the subtracted polarisation means this representation misses contributions from the heavy degrees of freedom that were integrated out in the formulation of the effective Lagrangian.

It is also worth considering the physics encoded in the term proportional to the NLO

LEC L_9^r in the NNLO expression. This $\mathcal{O}(q^4)$ LEC is associated with the pion form factor for which a ChPT description is available and has the form, at one loop, [66]

$$F_\pi(q^2) = 1 + \frac{2L_9^r(\mu)}{f_\pi^2}q^2 - \frac{q^2}{96\pi^2 f_\pi^2}\left[A\big(\frac{m_\pi^2}{q^2}, \frac{m_\pi^2}{\mu^2}\big) + \frac{1}{2}A\big(\frac{m_K^2}{q^2}, \frac{m_K^2}{\mu^2}\big)\right] \tag{5.30}$$

where

$$A\big(\frac{m^2}{q^2}, \frac{m^2}{\mu^2}\big) = \ln\big(m^2/\mu^2\big) + \frac{8m^2}{q^2} - \frac{5}{3} + (1 - 4m^2/q^2)^{3/2} \ln \frac{\sqrt{1 - 4m^2/q^2} + 1}{\sqrt{1 - 4m^2/q^2} - 1}. \tag{5.31}$$

The contribution of the vector meson ρ dominates the pion form factor. Using a chiral effective theory which is extended to include the octet of lightest vector resonances, a corresponding expression for the pion form factor is given by

$$F(q^2)_V = 1 + \frac{F_V G_V}{f_\pi^2}\frac{q^2}{m_\rho^2 - q^2}. \tag{5.32}$$

This offers an $\mathcal{O}(q^4)$ prediction for the LEC L_9^r [82]

$$L_9^r = \frac{f_\pi^2}{2m_\rho^2} \sim 7.2 \times 10^{-3} \tag{5.33}$$

which is a reasonable approximation to the result, $L_9^r = 5.93 \times 10^{-3}$, obtained in Ref. [79] and used in this work. The domination of the ρ contribution shown here is consistent with our expectation that the LECs in the chiral expansion beyond leading order are saturated by the effects of the heavy fields and will therefore play a dominant role in a_μ^{SIB}. The resonances in the ρ region contribute to the SIB correction through ρ-ω mixing (discussed in section 5.7), though we should emphasise that the contributions from a range of yet-heavier degrees of freedom present in the full QCD theory also, in principle, contribute to a_μ^{SIB}.

Despite this appearance of physics from full QCD in the NNLO prediction through the presence of the term proportional to L_9^r, this contribution is suppressed at NNLO through

multiplication by the loop function $\bar{B}(\bar{M}_K^2, Q^2)$. This corresponds to the embedding of the SIB resonance physics within a loop diagram rather than as a single vertex in the effective theory. A specific example of what is missing is a representation of the effect of $\rho-\omega$ mixing, which, in the full and effective theories would be represented by the following diagrams:

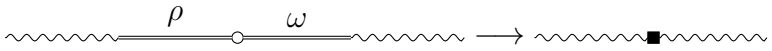

where the circle in the diagram explicitly containing ρ and ω represents the mixing of the two mesons, while the black square is the corresponding effective vertex encoding this contribution at some higher order in ChPT. We expect such a term to arise at higher order in the chiral Lagrangian and to generate a significant correction to the NNLO prediction. Our analysis in the following sections validates this statement predicated on assumptions laid out therein.

5.5 Inclusion of Effects at NNNLO in the Chiral Expansion

The dominant contribution to the full leading-order hadronic part of the anomalous magnetic moment, a_μ^{LO-HVP}, comes from the broad ρ resonance. Based on the discussion above, we also expect an important contribution to a_μ^{SIB} to come from ρ-ω mixing. However, since the ρ and ω were integrated out in constructing the effective chiral Lagrangian, there are no explicit appearances of such a ρ-ω mixing contribution in the NNLO prediction of the isospin breaking vector correlator. The effects of the heavy fields are condensed into the LECs of the chiral expansion and therefore the success of our prediction is crucially dependent on capturing the most significant of the LECs relevant to SIB in $\hat{\Pi}^{38}(Q^2)$.

The extent to which our ChPT prediction encompasses the LECs of greatest significance concerns the convergence of the chiral series at NNLO. In Ref. [72] it was shown that the NNLO piece of $\Pi^{38}(q^2)$ is greater in size than the NLO piece, even more so in the unsubtracted version, where the term proportional to the $\mathcal{O}(q^6)$ LEC $\hat{Q}^r$ ($\propto C_{61}$) is numerically

dominant. As previously mentioned, $\hat{Q}^r$ drops out when we go to the subtracted form of the polarisation function. Whilst one is unable to determine the convergence of the chiral series by solely comparing the relative sizes of the NLO and NNLO contributions, it is very likely from both the lack of $\mathcal{O}(q^6)$ LECs and the discrepancy between our NNLO prediction for a_μ^{SIB} and those of the aforementioned LQCD studies that even at two-loops ChPT does not offer a successful description of the dominant SIB processes.

It is not currently possible to extend our analysis to a full NNNLO evaluation of $\Pi^{38}(q^2)$. We may, however, follow the assumption made in Ref. [83] that for a typical resonance region choice of ChPT renormalisation scale such as $\mu = m_\rho$ the NNNLO contribution will be dominated by its tree-level components. With this assumption, we can identify the most significant piece of the full NNNLO contribution and use it to enhance our current prediction. This approach has also been previously employed in continuum and lattice chiral analyses.

In Ref. [83], the NNNLO LEC we require was determined using inverse-moment finite-energy sum rule (IMFESR) analyses of the flavour ud and us vector current two-point functions. The IMFESRs in question employed weights of the form $w(s)/s^2$ with $w(s)$ a polynomial, and hence analytic for all s. The products $\Pi_{ud,us;V}\, w(s)/s^2$ are integrated over the IMFESR contour consisting of a line extending from $s = s_0$ to 0 along the bottom of the physical cut in the ud, us polarisations, a line from 0 to $s = s_0$ above the same cut, closed by the circle $|s| = s_0$. The contributions to the contour integral from the integrals along the two sides of the physical cut are determined using hadronic τ decay data and the contribution from integral around the circle by using the operator product expansion for the ud and us polarisations. Since the only singularity inside this resulting closed contour is that produced by the $1/s^2$ factor, the results obtained in this way for the full contour integral, allow one to determine the derivatives of $\Pi_{ud,us;V}(Q^2)$ with respect to Q^2 at $Q^2 = 0$. These derivatives have NNLO ChPT representations involving known masses, known NLO LECs, and a term $8C_{93}^r$, involving the NNLO LEC C_{93}^r [73]. C_{93}^r can

thus be determined independently from both the ud and us IMFESRs. Were the NNLO representations to be well converged, these two values should be in good agreement. The fact that they are not [83] implies the existence of non-negligible NNNLO contributions to the representation of one or both of $\Pi_{ud;V}$ and $\Pi_{us;V}$. As pointed out in Ref. [83], there are only two possible terms in the NNNLO effective Lagrangian that would produce NNNLO contributions to $\Pi_{ud;V}$ and $\Pi_{us;V}$. only one of which contributes to the difference between the slopes with respect to Q^2 at $Q^2 = 0$ of these two polarisations. Ref. [83] introduced two NNNLO LECs $\delta C_{93}^{(1)}$ and $\delta C_{93}^{(2)}$ to parameterise the NNLO tree-level contributions to these slopes. Of these, it is $\delta C_{93}^{(1)}$ which contributes to the difference of the flavor ud and us slopes. The relevant quark-mass-dependent NNNLO term in the chiral Lagrangian is

$$\mathcal{L}_8 \sim \delta C_{93}^{(1)} \langle U^\dagger \chi O_{L,93} + \chi U^\dagger O_{R,93} \rangle \tag{5.34}$$

where

$$O_{L,R\,93} = D_\rho F_{L,R\,\mu\nu} D^\rho F_{L,R}^{\mu\nu} \, . \tag{5.35}$$

Since we are interested only in vector current two-point functions, we can readopt the formulation of ChPT in the presence of external vector sources only used in calculating Π^{38} by setting $\ell^\mu = r^\mu = v^\mu$ in the expressions for $F_L^{\mu\nu}$, $F_R^{\mu\nu}$ and the covariant derivative D_μ.

The resulting expression simplifies in momentum space. With $\chi = 2B_0\mathcal{M}$ and (since we are interested only in the NNNLO contribution produced by this term) the operator $U^\dagger$ expanded only to leading order, at which it is simply the unit matrix, we find

$$\mathcal{L}_8 \sim 4q^2 \delta C_{93}^{(1)} (q_\mu q_\nu - g_{\mu\nu} q^2) \langle 2B_0 \mathcal{M} v^\mu v^\nu \rangle. \tag{5.36}$$

From here one takes derivatives with respect to $v^{3\sigma}$ and $v^{8\lambda}$ to find the contribution to the $\sigma\lambda$ part of the 38 vector correlator. The resulting contribution to the vacuum polarisation

Π^{38} in terms of Euclidean Q^2 is

$$[\Pi^{38}(Q^2)]_{NNNLO} = -\frac{8Q^2}{2\sqrt{3}}\delta C_{93}^{(1)}(M_{K^0}^2 - M_{K^+}^2)_{QCD}. \tag{5.37}$$

Converting this result to the SIB part of the electromagnetic current polarisation finally leaves us with an NNNLO correction to our earlier result of

$$[\Pi^{SIB}(Q^2)]_{NNNLO} = -\frac{8Q^2}{3}\delta C_{93}^{(1)}(M_{K^0}^2 - M_{K^+}^2)_{QCD}. \tag{5.38}$$

The complete new NNLO plus tree-level NNNLO expression for the SIB component of the electromagnetic vacuum polarisation is given by

$$\begin{aligned}\hat{\Pi}^{SIB}(Q^2) =& \frac{1}{2}(M_{K^0}^2 - M_{K^+}^2)_{QCD}\times \\ & \Bigg[-\frac{1}{48\pi^2\bar{M}_K^2} + \frac{2i\bar{B}(\bar{M}_K^2, Q^2)}{Q^2}\Bigg\{1- \\ & \frac{2Q^2}{f^2}\left(2L_9^r(\mu) - i(\bar{B}_{21}(M_\pi^2, Q^2) + 2\bar{B}_{21}(\bar{M}_K^2, Q^2)) - \frac{1}{192\pi^2}\log\frac{M_\pi^2\bar{M}_K^4}{\mu^6}\right)\Bigg\} \\ & \frac{16}{3}Q^2\delta C_{93}^{(1)}\Bigg]\end{aligned} \tag{5.39}$$

The results for a_μ^{SIB} for this prediction are shown in Fig. 5.4 where for the numerical value of $\delta C_{93}^{(1)}$ we use the result denoted 'ACLP' from Eq. (4.15) in Ref. [83][1]

$$\delta C_{93}^{(1)} = 0.0239\,(27)\,\text{GeV}^{-4}. \tag{5.40}$$

[1]Two possible results are quoted for $\delta C_{93}^{(1)}$ in Ref. [83], differing in their choice of experimental *us* hadronic τ decay input. Since the original publication, new BaBar results for $\tau^- \to K^-\pi^0\nu_\tau$ have produced a reassessment of the HFLAV result for this branching fraction [84]. According to the authors of Ref. [83], this new result resolves the previous two-fold determination of $\delta C_{93}^{(1)}$ in favour of the 'ACLP' result.

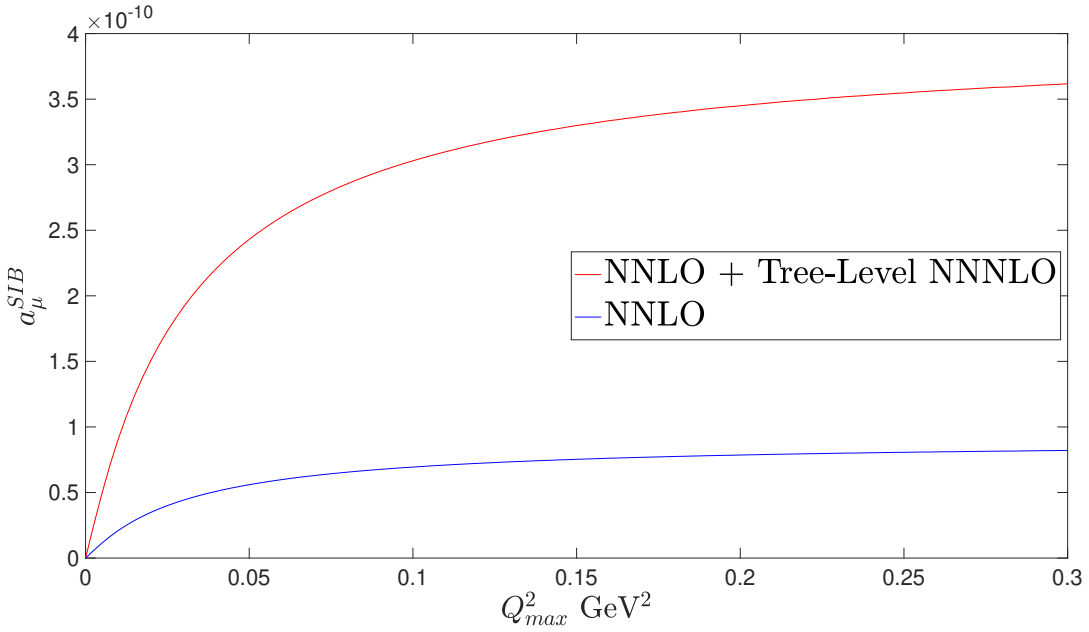

Figure 5.4: Results for the NNLO plus tree-level NNNLO prediction at values of the integration cutoff Q^2_{max} up to m^2_η.

5.6 NNLO plus Tree-Level NNNLO Results

At the cutoff $Q^2_{max} = m^2_\eta$ our NNLO plus tree-level NNNLO (TL-NNNLO) ChPT prediction for the SIB contribution to a_μ is

$$a_\mu^{SIB}\Big|_{NNLO+(TL)NNNLO} = 3.61(33) \times 10^{-10} \tag{5.41}$$

where the error is determined by summing in quadrature the 1σ error contributions to a_μ^{SIB} of the leading uncertainties in the NNLO expression, those of L^r_9, f, and the Dashen's theorem violation parameter ϵ, and the NNNLO uncertainty from $\delta C^{(1)}_{93}$. This result is within 1σ of the error bar of the aforementioned most precise Lattice determination of a_μ^{SIB} by the ETM collaboration.

Our results for the ChPT prediction extended to include the tree-level NNNLO LEC $\delta C^{(1)}_{93}$ reveal that ChPT receives significant corrections to the leading-order SIB component of the EM vacuum polarisation beyond NNLO. As expected the uncertainty in our determination is similarly dominated by the NNNLO LEC. Fig. 5.5 overlays error bands

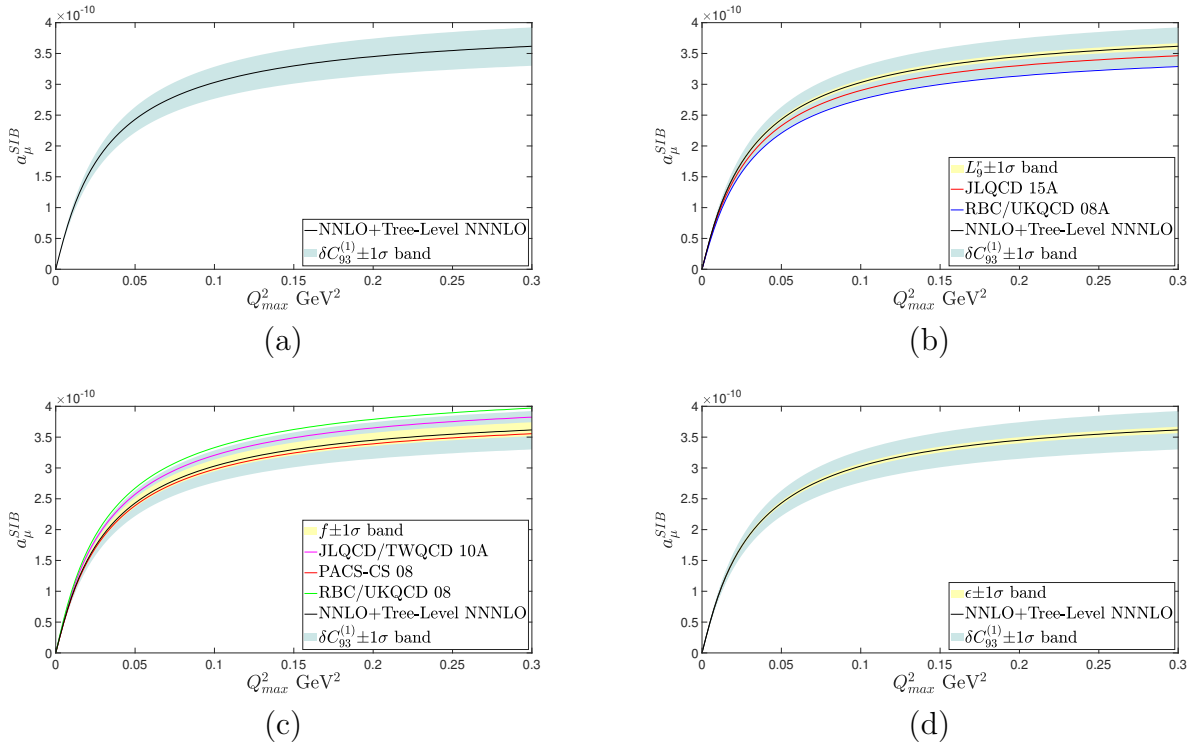

Figure 5.5: Comparison of the size of the largest NNLO uncertainties with that produced by the uncertainty in $\delta C_{93}^{(1)}$. (a) The NNLO plus tree-level NNNLO results showing the error band arising from the uncertainty in the value of $\delta C_{93}^{(1)}$ only. In the remaining plots this is compared to (b) the error band for our value of L_9^r and results using the central values of L_9^r from JLQCD 15A [4] and RBC/UKQCD 08A [5] (c) the error band for f and results using the central values of f from JLQCD/TWQCD 10A [6], PACS-CS 08 [7], and RBC/UKQCD [8] (d) the error band for ϵ of Eq. 5.21.

associated with the leading uncertainties in the NNLO expression, specifically those in L_9^r, f, and ϵ, with the error band associated with the uncertainty in $\delta C_{93}^{(1)}$. In addition results are shown using alternate determinations of the parameters L_9^r and f given in the 2019 FLAG review [69]. Where groups have recorded multiple values for these constants, the most recent was chosen. In the case of ϵ, the FLAG review presents a result which averages the determinations by RM123 17 [85] and BMW 14 [86], and we therefore present the error band associated with the average, rather than the separate results.

The analyses using the RBC/UKQCD values returned results slightly outside the $\delta C_{93}^{(1)}\pm 1\sigma$ error band in both the L_9^r and f cases (plots (b) and (c) of Fig. 5.5). In Fig. 5.6 the separate analyses using the RBC/UKQCD values are plotted with 1σ error bands which

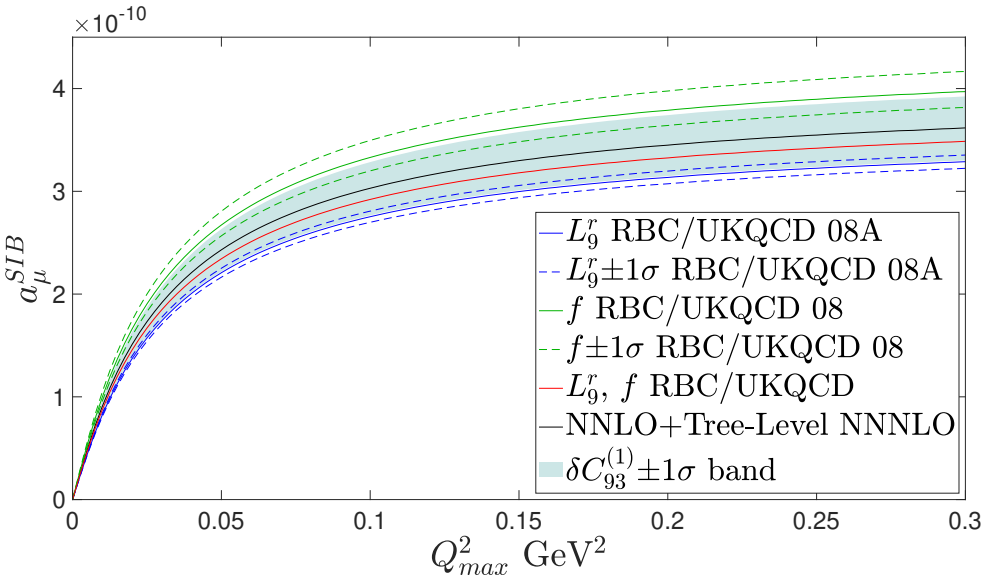

Figure 5.6: The 1σ error bands associated with the RBC/UKQCD 08/08A determinations of the constants L_9^r and f. The error bands are shown for separate analyses using only one of either the RBC/UKQCD values for L_9^r and f. Also shown are the results using both RBC/UKQCD input values (red line).

are found to overlap with the $\delta C_{93}^{(1)} \pm 1\sigma$ region. Also plotted is the result of an analysis using the RBC/UKQCD values for both f and L_9^r. This result was found to lie well inside the $\delta C_{93}^{(1)} \pm 1\sigma$ region.

These plots demonstrate the dominance of the uncertainty in $\delta C_{93}^{(1)}$ in the overall error of the NNLO plus tree-level NNNLO prediction. In the next section we interpret this finding by considering the nature of the dominant SIB processes and the role of resonance physics in the effective chiral framework.

5.7 Interpretation of the NNNLO Contribution

It is known that the LECs of ChPT at NLO, evaluated at a renormalisation scale $\mu \simeq m_\rho$, are saturated by contributions from the lowest energy resonances [87, 88]. As previously discussed, the effects of ρ-ω mixing are expected to play an important role in determining the SIB component of the LO HVP. Precision measurements of the pion form factor, $F_\pi(s)$, arising from studies of the $e^+e^- \to \pi^+\pi^-$ process (Fig 5.8) offer experimentally

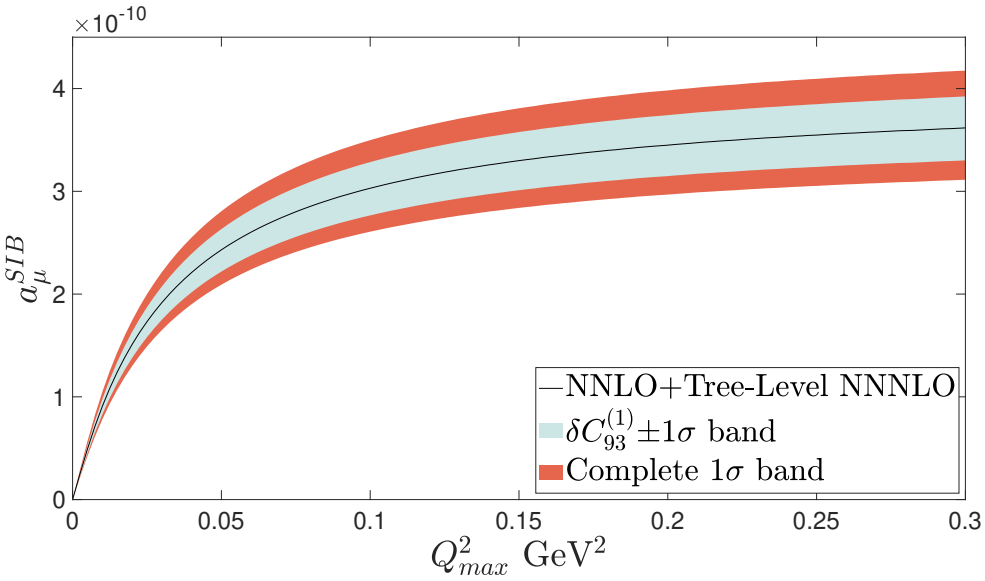

Figure 5.7: Error bands for the NNLO plus tree-level NNNLO result from (blue) the uncertainty in $\delta C_{93}^{(1)}$, and (red) the combined $\pm 1\sigma$ for $\delta C_{93}^{(1)}, f, L_9^r, \epsilon$, where the band limits are set by the maximum/minimum 1σ values of these quantities.

accessible data on this mixing phenomenon. Interest in the experimental determination of $F_\pi(s)$ has been fueled by the dominance of the $\pi\pi$ contribution to the HVP in dispersive determinations of the LO-HVP contribution to a_μ. Furthermore, isospin breaking in the resonance region is important to studies of charge symmetry breaking in the NN interaction [89].

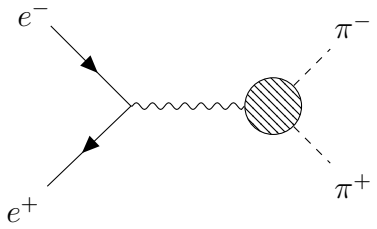

Figure 5.8: The pion form factor (shaded circle) in the $e^+e^- \to \pi^+\pi^-$ interaction.

There exist a range of models describing the ρ-ω interference contribution to the $e^+e^- \to \pi^+\pi^-$ amplitude (see Ref. [90] and references therein). In each case the model dependence of the $\rho - \omega$ mixing dominates over the induced uncertainties by experimental errors. For the purposes of this discussion we may draw upon the success of vector meson dominance (VMD) in describing the pion form factor [91].

VMD has it origins in Nambu's suggestion that the charge distribution for protons and neutrons determined through electron scattering can be explained by the contribution of heavy vector mesons to the nucleon form factor. The VMD description assumes that the components of the HVP are dominated by the contributions from the known vector mesons. ρ-ω mixing in the VMD framework is described in Refs. [92, 93].

Based on the observation that mixing of the ρ and ω is small, the transformation between the physical and pure isospin states can be approximated by

$$|\rho\rangle = |\rho_I\rangle - \epsilon_1|\omega_I\rangle \tag{5.42}$$

$$|\omega\rangle = |\omega_I\rangle + \epsilon_2|\rho_I\rangle \tag{5.43}$$

where ϵ_1 and ϵ_2 are small, complex mixing parameters which are in general only equal when the mixing becomes independent of the momentum-squared, which is a special case restricted to the region near the ω mass.

One may consider the vector meson propagator,

$$D_{\mu\nu}(q^2) = \int d^4x e^{-iq\cdot x}\langle 0|V_\mu(x)V_\nu(0)|0\rangle \tag{5.44}$$

which in the context of conserved currents coupled to vector mesons can be converted to the scalar propagator via $D_{\mu\nu}(q^2) = -g_{\mu\nu}D(q^2)$. The $\rho-\omega$ mixing piece of the propagator is given by [94]

$$D^I_{\rho\omega} = \frac{\Pi_{\rho\omega}(q^2)}{(q^2 - m_\rho^2 - \Pi^{(0)}_{\rho\rho}(q^2))(q^2 - m_\omega^2 - \Pi^{(0)}_{\omega\omega}(q^2))} \tag{5.45}$$

According to Ref. [93], the mixing parameters ϵ_1, ϵ_2 are fixed by requiring the scalar propagator $D_{\rho\omega}(q^2)$ to contain no ρ or ω poles [93],

$$\epsilon_1 = \frac{\Pi_{\rho\omega}(m_\omega^2)}{m_\omega^2 - m_\rho^2 - \Pi^{(0)}_{\rho\rho}(m_\omega^2)} \tag{5.46}$$

$$\epsilon_2 = \frac{\Pi_{\rho\omega}(m_\rho^2)}{m_\omega^2 - m_\rho^2 - \Pi^{(0)}_{\omega\omega}(m_\rho^2)} \tag{5.47}$$

where $\Pi^{(0)}_{\alpha\alpha}(q^2) = \Pi_{\alpha\alpha}(q^2) - m_\alpha^2$ is a subtracted form of the renormalised self-energies. A Feynman diagram for the $\rho - \omega$ mixing contribution to the $e^+e^- \to \pi^+\pi^-$ process is shown in Fig. 5.9 where a photon couples to a vector meson as described in Ref. [92].

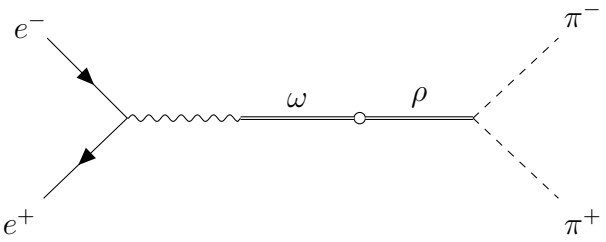

Figure 5.9: ω-ρ mixing in the $e^+e^- \to \pi^+\pi^-$ interaction. The circle between the ω and ρ propagators represents the possible hadronic physics contributing to their mixing.

In Ref. [90] a method of averaging over the various different models yielded a result for the contribution of ρ-ω mixing plus direct $\omega \to 2\pi$ coupling to the value of a_μ,

$$\delta a_\mu^{LO-HAD} = 3.1(1.5)_{model}(0.3)_{data} \times 10^{-10}. \tag{5.48}$$

In comparison, taking as an integration cutoff in our calculation $Q^2_{max} = m_\eta^2$, we find an increase between NNLO and NNLO plus tree-level NNNLO results of

$$\delta a_\mu^{SIB} = a_\mu^{SIB}\Big|_{\text{NNLO+TL-NNNLO}} - a_\mu^{SIB}\Big|_{\text{NNLO}} = 2.79(35) \times 10^{-10} \tag{5.49}$$

where the error given here is obtained by quadrature from the errors of the two ChPT results presented in this work. The 1σ consistency between the value of δa_μ^{LO-HAD} in Ref. [90] and our δa_μ^{SIB} strongly supports the conclusion that the dominant physical processes captured by the NNNLO LEC $\delta C_{93}^{(1)}$ are those involving the lightest resonances, in particular, ρ-ω mixing.

Two sources of potential uncertainty remain to be estimated in our results for a_μ^{SIB}, that associated with the truncation of the integral in Eq. 5.12 at $Q^2_{max} = m_\eta^2$ and that associated

with NNLO plus TL-NNNLO truncation of the low-energy representation of $\hat{\Pi}^{SIB}(Q^2)$. For the latter, with what is expected to be the dominant resonance-region contribution from ρ-ω mixing now incorporated through the TL-NNNLO contribution proportional to $\delta C_{93}^{(1)}$, we expect the standard $\sim 25\%$ SU(3) ChPT rule of thumb to provide a reasonable estimate for yet-higher order contributions. The estimated chiral-order-truncation uncertainty in our result for a_μ^{SIB} is then 0.9×10^{-10}. To estimate the former we note that, as discussed above, our results imply that the SIB contribution, like the isospin-conserving contribution, is dominated by contributions from the lowest lying vector meson region. We can thus use the behavior of the isospin-conserving contribution as a function of Q^2_{max} to estimate what fraction of the SIB contribution is omitted by truncating the integral at $Q^2_{max} = m^2_\eta$. This fraction is known for the isospin-conserving contribution as a result of the dispersive study of this contribution carried out in Ref. [95] for the I=1 flavour ud subtracted vacuum polarisation. In that study the subtracted $I-1$ polarisation is determined using a dispersive representation employing ud V channel hadronic tau decay data for the ud V spectral function [96]. The small contributions to $\Pi^{ud;V}(Q^2)$ from the region of Q^2 above the limits at which current data is available ($s > m^2_\tau$), are generated from a theoretical representation involving perturbative contributions plus duality violating contributions. Figure 2 of Ref. [95] shows the fraction of the I=1 component of the LO-HVP contribution to a_μ as a function of the Euclidean Q^2 integral cutoff, Q^2_{max}. The results of this study show that the truncation of the integral at 0.3 GeV$^2 \sim m^2_\eta$, as was done in our analysis, captures over 95% of the I=1 contribution to a_μ. Using this result, we estimate that missing contributions from the region of the integral above $Q^2 = m^2_\eta$ represent less than 5% of a_μ^{SIB}. The associated $Q^2 = m^2_\eta$-truncation uncertainty on a_μ^{SIB} is then 0.18×10^{-10}.

Combining these two additional uncertainties in quadrature with the uncertainty in

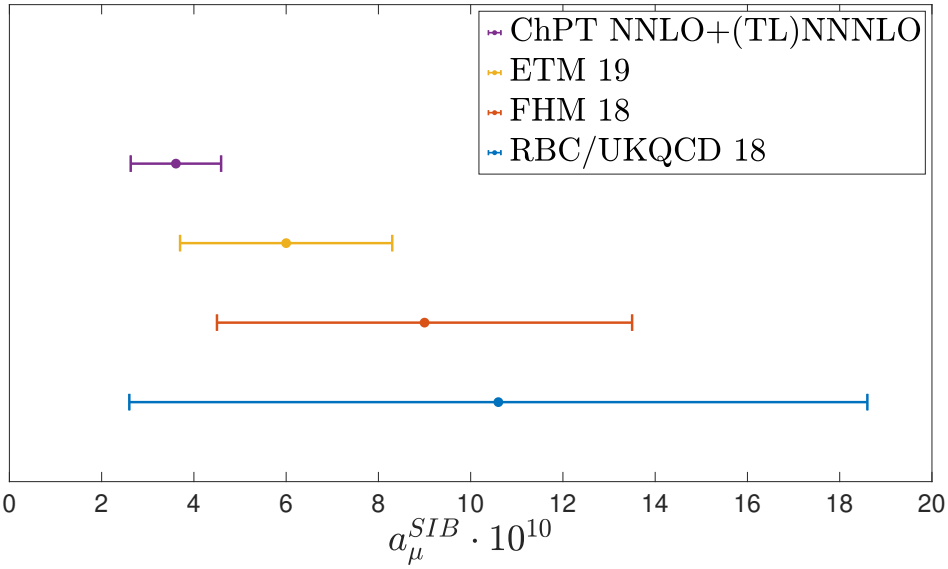

Figure 5.10: Compilation of results for a_μ^{SIB}. The values shown in addition to our ChPT result are: ETM 19 [9], RBC/UKQCD 18 [10, 11], FHM 18 [12].

Eq. 5.41, we arrive at our final result,

$$\begin{aligned} a_\mu^{SIB}\Big|_{NNLO+(TL)NNNLO} &= 3.61(33)(90)(18) \times 10^{-10} \\ &= 3.61(98) \times 10^{-10} \ . \end{aligned} \tag{5.50}$$

Chapter 6

Conclusion

The aim of this analysis was to make a quantitative prediction of the strong isospin breaking contribution to the value of the anomalous magnetic moment of the muon. This prediction was successfully obtained and found to be consistent with previous LQCD determinations. Furthermore, the estimated error was found to be smaller than that of the most precise of these previous LQCD results [9] shown in Fig. 5.10. The final value for a_μ^{SIB}, calculated using ChPT at NNLO plus tree-level NNNLO, and given in Eq. 5.50, represents a new non-perturbative determination of a_μ^{SIB}, intended to provide a useful target for future LQCD studies. In particular, the dominance by heavier resonance contributions ensures that Lattice finite volume effects should be small.

The results of the E989 experiment at Fermilab, and later the alternative J-PARC E34 experiment, are expected to provide a sharpened test of the SM, and an improved, precision-frontier search for signs of beyond-the-SM physics. In order to take full advantage of the anticipated experimental upgrade it is crucial that improvements to the prediction of the SM contribution to a_μ continue to be made. An important feature of the leading-order hadronic contribution to a_μ, which at present is responsible for the largest source of uncertainty in the current SM prediction, has been studied in this thesis. The results of this research offer clarification on the physical source of the dominant contributions to the

SIB contribution to this quantity, information that may be utilised in future research by LQCD groups.

The ChPT result and its consistency with independent contemporary LQCD analyses confirms the expectation that the SIB contribution is dominated by the low-momentum regime. The increase in size of the ChPT results from NNLO to tree-level NNNLO supports the conclusion that SIB resonance phenomena, such as ρ-ω mixing (discussed in Chapter 5), are responsible for the most significant part of a_μ^{SIB}. In the ChPT analysis these contributions are encoded in the term proportional to the LEC, $\delta C_{93}^{(1)}$, from the NNNLO effective chiral Lagrangian. As emphasised in the results section discussion, the full range of higher order QCD SIB effects play a role in determining the exact value of $\delta C_{93}^{(1)}$ at a particular renormalisation scale in the $\overline{\text{MS}}$ scheme. However, comparison with the predicted ρ-ω mixing contribution to a_μ^{HVP} from Ref. [90] supports the understanding that the light resonances are, indeed, responsible for the dominant contribution to a_μ^{SIB}.

The ChPT result predicts that SIB effects represent $\approx 0.5\%$ of the total hadronic contribution to a_μ, compatible with qualitative $\approx 1\%$ expectations for the size of such effects. With the LQCD community having set a target of 0.1% for the precision of future LQCD determinations of the LO-HVP contribution, previous LQCD studies, and now ChPT, independently establish that effects from SIB physics cannot be neglected in such determinations. The goal of this thesis has been to provide an improved prediction for this contribution, and hence aid in sharpening the precision with which the SM contribution to a_μ is known. Improvements of this type will play a vital role in determining whether new physics will be needed to explain the new experimental results.

The ChPT analysis is primarily limited by the increasing scale of calculations and unknown constants required to carry out an analysis to higher orders in the chiral expansion. However, given the consistency with LQCD results, and the evidence that the dominant physical effects have been incorporated in the current analysis, it is expected that uncertainties associated with higher-order contributions omitted in this analysis will have been

reliably taken into account by the error estimate presented above.

Future work in this area should continue to seek out constraints for the improvement of LQCD studies of the hadronic contributions to a_μ. Ongoing enhancements of the SM prediction will continue to provide an excellent opportunity to push the constraints on new physics at the precision frontier. The limiting uncertainties in the leading-order HVP and hadronic light-by-light scattering contribution predictions are being reduced by refinements to LQCD analyses, which are reaching levels competitive with results from methods based on QCD dispersion relations. The stage is set for future studies in light of the highly anticipated new experimental data to comprehensively understand the nature of the existing muon $g-2$ discrepancy.

References

[1] M Tanabashi et al. Review of Particle Physics. *Physical Review D*, 98(3):030001, Aug 2018.

[2] Stefan Scherer and Matthias R Schindler. *A primer for chiral perturbation theory*, volume 830. Springer Science & Business Media, 2011.

[3] Friedrich Jegerlehner. *The anomalous magnetic moment of the muon*, volume 274. Springer, 2017.

[4] Sinya Aoki, Guido Cossu, Xu Feng, Shoji Hashimoto, Takeshi Kaneko, J Noaki, and Tetsuya Onogi. Light meson electromagnetic form factors from three-flavor lattice QCD with exact chiral symmetry. *Physical Review D*, 93(3):034504, 2016.

[5] PA Boyle, JM Flynn, A Jüttner, C Kelly, H Pedroso de Lima, CM Maynard, CT Sachrajda, JM Zanotti, et al. The pion's electromagnetic form factor at small momentum transfer in full lattice QCD. *Journal of High Energy Physics*, 2008(07):112, 2008.

[6] H Fukaya, S Aoki, TW Chiu, S Hashimoto, T Kaneko, J Noaki, T Onogi, N Yamada, et al. Determination of the chiral condensate from QCD Dirac spectrum on the lattice. *Physical Review D*, 83(7):074501, 2011.

[7] S Aoki, K-I Ishikawa, N Ishizuka, T Izubuchi, D Kadoh, K Kanaya, Y Kuramashi, Y Namekawa, M Okawa, Y Taniguchi, et al. 2+1 flavor lattice QCD toward the physical point. *Physical Review D*, 79(3):034503, 2009.

[8] Chris Allton, DJ Antonio, Y Aoki, T Blum, PA Boyle, NH Christ, MA Clark, SD Cohen, C Dawson, MA Donnellan, et al. Physical results from 2+1 flavor domain wall QCD and SU(2) chiral perturbation theory. *Physical Review D*, 78(11):114509, 2008.

[9] D Giusti, V Lubicz, G Martinelli, F Sanfilippo, S Simula, ETM Collaboration, et al. Electromagnetic and strong isospin-breaking corrections to the muon g-2 from lattice QCD + QED. *Physical Review D*, 99(11):114502, 2019.

[10] Vera Gülpers, Andreas Jüttner, Christoph Lehner, and Antonin Portelli. Isospin breaking corrections to the HVP at the physical point. *arXiv preprint arXiv:1812.09562*, 2018.

[11] Johan Bijnens and Johan Relefors. Vector two-point functions in finite volume using partially quenched chiral perturbation theory at two loops. *Journal of High Energy Physics*, 2017(12):114, 2017.

[12] HPQCD Fermilab Lattice, MILC Collaborations, B Chakraborty, CTH Davies, C DeTar, AX El-Khadra, E Gámiz, Steven Gottlieb, D Hatton, J Koponen, et al. Strong-isospin-breaking correction to the muon anomalous magnetic moment from lattice QCD at the physical point. *Physical Review Letters*, 120(15):152001, 2018.

[13] Salvatore Rappoccio. The experimental status of direct searches for exotic physics beyond the Standard Model at the Large Hadron Collider. *Reviews in Physics*, page 100027, 2018.

[14] Paul Adrien Maurice Dirac. The quantum theory of the electron. *Proceedings of the Royal Society of London. Series A, Containing Papers of a Mathematical and Physical Character*, 117(778):610–624, 1928.

[15] Tatsumi Aoyama, Toichiro Kinoshita, and Makiko Nio. Theory of the Anomalous Magnetic Moment of the Electron. *Atoms*, 7(1):28, 2019.

[16] DELPHI collaboration et al. Study of tau-pair production in photon-photon collisions at LEP and limits on the anomalous electromagnetic moments of the tau lepton. *The European Physical Journal C-Particles and Fields*, 35(2):159–170, 2004.

[17] S Eidelman and M Passera. Theory of the τ lepton anomalous magnetic moment. *Modern Physics Letters A*, 22(03):159–179, 2007.

[18] Lydia Beresford and Jesse Liu. New physics and tau $g-2$ using LHC heavy ion collisions. *arXiv preprint arXiv:1908.05180*, 2019.

[19] David W Hertzog, James P Miller, Eduardo De Rafael, B Lee Roberts, and Dominik Stockinger. The physics case for the new muon (g-2) experiment. *arXiv preprint arXiv:0705.4617*, 2007.

[20] J Grange, V Guarino, P Winter, K Wood, H Zhao, RM Carey, D Gastler, E Hazen, N Kinnaird, JP Miller, et al. Muon (g-2) technical design report. 2015.

[21] Fermilab Muon g-2 Collab, http://muon-g-2.fnal.gov.

[22] M Abe, S Bae, G Beer, G Bunce, H Choi, S Choi, M Chung, W Da Silva, S Eidelman, M Finger, et al. A new approach for measuring the muon anomalous magnetic moment and electric dipole moment. *Progress of Theoretical and Experimental Physics*, 2019(5):053C02, 2019.

[23] J-PARC g-2/EDM Collab, http://g-2.kek.jp.

[24] Gerald W Bennett, B Bousquet, HN Brown, G Bunce, RM Carey, P Cushman, GT Danby, PT Debevec, M Deile, H Deng, et al. Final report of the E821 muon anomalous magnetic moment measurement at BNL. *Physical Review D*, 73(7):072003, 2006.

[25] Thomas Blum, PA Boyle, V Gülpers, T Izubuchi, L Jin, C Jung, A Jüttner, C Lehner, A Portelli, JT Tsang, et al. Calculation of the hadronic vacuum polarization

contribution to the muon anomalous magnetic moment. *Physical Review Letters*, 121(2):022003, 2018.

[26] Kohtaroh Miura. Review of Lattice QCD studies of hadronic vacuum polarization contribution to muon g-2. *arXiv preprint arXiv:1901.09052*, 2019.

[27] Georges Charpak, FJM Farley, Richard L Garwin, Th Muller, Johannes C Sens, and A Zichichi. A new measurement of the anomalous magnetic moment of the muon. *Physics Letters*, 1:16–20, 1962.

[28] J Bailey, K Borer, F Combley, H Drumm, FJM Farley, JH Field, W Flegel, PM Hattersley, F Krienen, F Lange, et al. The anomalous magnetic moment of positive and negative muons. *Physics Letters B*, 68(2):191–196, 1977.

[29] J Bailey, K Borer, F Combley, H Drumm, C Eck, FJM Farley, JH Field, W Flegel, PM Hattersley, F Krienen, et al. Final report on the CERN muon storage ring including the anomalous magnetic moment and the electric dipole moment of the muon, and a direct test of relativistic time dilation. *Nuclear Physics B*, 150:1–75, 1979.

[30] Ran Hong. Magnetic field measurement and analysis for the muon g-2 experiment. *arXiv preprint arXiv:1909.13742*, 2019.

[31] AT Fienberg. The status and prospects of the muon $g-2$ experiment at Fermilab. *arXiv preprint arXiv:1905.05318*, 2019.

[32] Tatsumi Aoyama, Masashi Hayakawa, Toichiro Kinoshita, and Makiko Nio. Complete tenth-order QED contribution to the muon g-2. *Physical Review Letters*, 109(11):111808, 2012.

[33] Tatsumi Aoyama, Masashi Hayakawa, Toichiro Kinoshita, and Makiko Nio. Tenth-order QED contribution to the electron $g-2$ and an improved value of the fine structure constant. *Phys. Rev. Lett.*, 109:111807, Sep 2012.

[34] Friedrich Jegerlehner. Muon g–2 theory: The hadronic part. In *EPJ Web of Conferences*, volume 166, page 00022. EDP Sciences, 2018.

[35] Johan Bijnens. On the hadronic light-by-light contribution to the muon g–2. In *EPJ Web of Conferences*, volume 179, page 01001. EDP Sciences, 2018.

[36] Massimiliano Procura, Peter Stoffer, Martin Hoferichter, and Gilberto Colangelo. Hadronic contributions to the muon anomalous magnetic moment. *PoS*, 336:186, 2019.

[37] Nils Asmussen, Antoine Gérardin, Andreas Nyffeler, and Harvey B Meyer. Hadronic light-by-light scattering in the anomalous magnetic moment of the muon. In *Proceedings for the 15th International Workshop on Tau Lepton Physics*, volume 24, page 28, 2018.

[38] Rende Steerenberg. LHC status and outlook to the HL-LHC. 2019.

[39] Michael Benedikt and Frank Zimmermann. Status of the future circular collider study. Technical report, FCC-DRAFT-ACC-2016-030, 2016.

[40] VB Berestetskii, ON Krokhin, and AX Klebnikov. *Sov. Phys. JETP*, 3:761, 1956.

[41] WS Cowland. On Schwinger's theory of the muon. *Nuclear Physics*, 8:397–401, 1958.

[42] Matthew D Schwartz. *Quantum field theory and the Standard Model*. Cambridge University Press, 2014.

[43] Michael E Peskin and D V Schoeder. *An introduction to quantum field theory*. CRC Press, 2018.

[44] Freeman J Dyson. The radiation theories of Tomonaga, Schwinger, and Feynman. *Physical Review*, 75(3):486, 1949.

[45] C Gnendiger, D Stöckinger, and H Stöckinger-Kim. The electroweak contributions to (g-2)$_\mu$ after the Higgs-boson mass measurement. *Physical Review D*, 88(5):053005, 2013.

[46] Martin L Perl, Eric R Lee, and Dinesh Loomba. A brief review of the search for isolatable fractional charge elementary particles. *Modern Physics Letters A*, 19(35):2595–2610, 2004.

[47] István Montvay and Gernot Münster. *Quantum fields on a lattice*. Cambridge University Press, 1997.

[48] Carleton DeTar et al. *Lattice methods for quantum chromodynamics*. World Scientific, 2006.

[49] J Smit. Introduction to quantum fields on a lattice: A robust mate. *Cambridge Lect. Notes Phys.*, 15:1–271, 2002.

[50] Claudia Ratti. Lattice QCD and heavy ion collisions: a review of recent progress. *Reports on Progress in Physics*, 81(8):084301, 2018.

[51] Eduardo de Rafael. An introduction to sum rules in QCD. *arXiv preprint hep-ph/9802448*, 1998.

[52] Roman Zwicky. A brief introduction to dispersion relations and analyticity. *arXiv preprint arXiv:1610.06090*, 2016.

[53] M Gourdin and E De Rafael. Hadronic contributions to the muon g-factor. *Nuclear Physics B*, 10(4):667–674, 1969.

[54] Stanley J Brodsky and Eduardo De Rafael. Suggested boson-lepton pair couplings and the anomalous magnetic moment of the muon. *Physical Review*, 168(5):1620, 1968.

[55] M Davier, A Hoecker, B Malaescu, and Z Zhang. A new evaluation of the hadronic vacuum polarisation contributions to the muon anomalous magnetic moment and to $\alpha(m_z^2)$. *arXiv preprint arXiv:1908.00921*, 2019.

[56] B. Aubert, Y. Karyotakis, J. P. Lees, V. Poireau, E. Prencipe, X. Prudent, V. Tisserand, J. Garra Tico, E. Grauges, M. Martinelli, and et al. Precise measurement of the $e^+e \to \pi^+\pi^-(\gamma)$ cross section with the initial state radiation method at BABAR. *Physical Review Letters*, 103(23), Dec 2009.

[57] J. P. Lees, V. Poireau, V. Tisserand, J. Garra Tico, E. Grauges, A. Palano, G. Eigen, B. Stugu, D. N. Brown, L. T. Kerth, and et al. Precise measurement of the $e^+e^- \to \pi^+\pi^-(\gamma)$ cross section with the initial-state radiation method at BABAR. *Physical Review D*, 86(3), Aug 2012.

[58] F Ambrosino, A Antonelli, M Antonelli, F Archilli, C Bacci, P Beltrame, G Bencivenni, S Bertolucci, C Bini, C Bloise, et al. Measurement of $\sigma(e^+e^- \to \pi^+\pi^-\gamma(\gamma))$ and the dipion contribution to the muon anomaly with the KLOE detector. *Physics Letters B*, 670(4-5):285–291, 2009.

[59] F Ambrosino, F Archilli, P Beltrame, G Bencivenni, C Bini, C Bloise, S Bocchetta, F Bossi, P Branchini, G Capon, et al. Measurement of $\sigma(e^+e^- \to \pi^+\pi^-)$ from threshold to 0.85 GeV^2 using initial state radiation with the KLOE detector. *Physics Letters B*, 700(2):102–110, 2011.

[60] D Babusci, D Badoni, I Balwierz-Pytko, G Bencivenni, C Bini, C Bloise, F Bossi, P Branchini, A Budano, L Caldeira Balkeståhl, et al. Precision measurement of $\sigma(e^+e^- \to \pi^+\pi^-\gamma)/\sigma(e^+e^- \to \mu^+\mu^-\gamma)$ and determination of the π^+ π^- contribution to the muon anomaly with the KLOE detector. *Physics Letters B*, 720(4-5):336–343, 2013.

[61] T Blum. Lattice calculation of the lowest-order hadronic contribution to the muon anomalous magnetic moment. *Physical Review Letters*, 91(5):052001, 2003.

[62] Aneesh V Manohar. Effective field theories. In *Perturbative and nonperturbative aspects of quantum field theory*, pages 311–362. Springer, 1977.

[63] Cliff P Burgess. An introduction to effective field theory. *Ann. Rev. Nucl. Part. Sci.*, 57:329–362, 2007.

[64] Aneesh V Manohar. Introduction to effective field theories. *arXiv preprint arXiv:1804.05863*, 2018.

[65] Jürg Gasser and Heinrich Leutwyler. Chiral perturbation theory to one loop. *Annals of Physics*, 158(1):142–210, 1984.

[66] Jürg Gasser and Heinrich Leutwyler. Chiral perturbation theory: expansions in the mass of the strange quark. *Nuclear Physics B*, 250(1-4):465–516, 1985.

[67] Steven Weinberg. Phenomenological Lagrangians. *Physica A: Statistical Mechanics and its Applications*, 96(1):327 – 340, 1979.

[68] Jeffrey Goldstone, Abdus Salam, and Steven Weinberg. Broken Symmetries. *Phys. Rev.*, 127:965–970, Aug 1962.

[69] S Aoki, Y Aoki, D Becirevic, T Blum, G Colangelo, S Collins, M Della Morte, P Dimopoulos, S Dürr, H Fukaya, et al. FLAG review 2019. *arXiv preprint arXiv:1902.08191*, 2019.

[70] Johan Bijnens, Gilberto Colangelo, and Gerhard Ecker. The mesonic chiral Lagrangian of order p^6. *Journal of High Energy Physics*, 1999(02):020, 1999.

[71] Johan Bijnens, Nils Hermansson-Truedsson, and Si Wang. The order p^8 mesonic chiral lagrangian. *Journal of High Energy Physics*, 2019(1):102, 2019.

[72] Kim Maltman. The vector current correlator $\langle 0|T(V_\mu^3 V_\nu^8)|0\rangle$ to two loops in chiral perturbation theory. *Physical Review D*, 53:2573–2585, 03 1996.

[73] Gabriel Amorós, Johan Bijnens, and Pere Talavera. Two-point functions at two loops in three flavour chiral perturbation theory. *Nuclear Physics B*, 568(1-2):319–363, 2000.

[74] Eugene Golowich and Joachim Kambor. Two-loop analysis of vector-current propagators in chiral perturbation theory. *Nuclear Physics B*, 447(2-3):373–404, 1995.

[75] Giampiero Passarino and Martinus Veltman. One-loop corrections for e^+ e^- annihilation into μ^+ μ^- in the Weinberg model. *Nuclear Physics B*, 160(1):151–207, 1979.

[76] Gerard 't Hooft and M. J. G. Veltman. Regularization and Renormalization of Gauge Fields. *Nucl. Phys.*, B44:189–213, 1972.

[77] Maarten Golterman, Kim Maltman, and Santiago Peris. NNLO low-energy constants from flavor-breaking chiral sum rules based on hadronic τ-decay data. *Physical Review D*, 89:054036, Mar 2014.

[78] Maarten Golterman, Kim Maltman, and Santiago Peris. Chiral LECs from flavor-breaking inverse moment finite energy sum analyses of hadronic τ decay data. *Nuclear and Particle Physics Proceedings*, 260:125–129, 2015.

[79] Johan Bijnens and Pere Talavera. Pion and kaon electromagnetic form factors. *Journal of High Energy Physics*, 2002(03):046, 2002.

[80] A Bazavov, C Bernard, C DeTar, X Du, W Freeman, Steven Gottlieb, Urs M Heller, JE Hetrick, J Laiho, L Levkova, et al. Results for light pseudoscalar mesons. *arXiv preprint arXiv:1012.0868*, 2010.

[81] Gilberto Colangelo, Stephan Dürr, Andreas Jüttner, Laurent Lellouch, Heinrich Leutwyler, Vittorio Lubicz, Silvia Necco, Christopher T Sachrajda, Silvano Simula, Anastassios Vladikas, et al. Review of lattice results concerning low-energy particle physics. *The European Physical Journal C*, 71(7):1695, 2011.

[82] Francisco Guerrero and Antonio Pich. Effective field theory description of the pion form factor. *Physics Letters B*, 412(3-4):382–388, 1997.

[83] Maarten Golterman, Kim Maltman, and Santiago Peris. Determination of the NNLO low-energy constant C_{93}. *Physical Review D*, 96(5):054027, 2017.

[84] Gerald Eigen. Recent results on *tau* decays. *arXiv preprint arXiv:1906.12232*, 2019.

[85] D Giusti, V Lubicz, C Tarantino, G Martinelli, F Sanfilippo, S Simula, N Tantalo, RM123 Collaboration, et al. Leading isospin-breaking corrections to pion, kaon, and charmed-meson masses with twisted-mass fermions. *Physical Review D*, 95(11):114504, 2017.

[86] Sz Borsanyi, S Durr, Zoltán Fodor, C Hoelbling, SD Katz, S Krieg, L Lellouch, T Lippert, A Portelli, KK Szabo, et al. Ab initio calculation of the neutron-proton mass difference. *Science*, 347(6229):1452–1455, 2015.

[87] Gerhard Ecker, Jürg Gasser, Antonio Pich, and Eduardo De Rafael. The role of resonances in chiral perturbation theory. *Nuclear Physics B*, 321(2):311–342, 1989.

[88] John F Donoghue, Carlos Ramirez, and German Valencia. Spectrum of QCD and chiral Lagrangians of the strong and weak interactions. *Physical Review D*, 39(7):1947, 1989.

[89] Gerald A Miller, Allena K Opper, and Edward J Stephenson. Charge symmetry breaking and QCD. *Ann. Rev. Nucl. Part. Sci.*, 56:253–292, 2006.

[90] Carl E Wolfe and Kim Maltman. Models of isospin breaking in the pion form factor: Consequences for the determination of $\Pi_{\rho\omega}(m_\rho^2)$ and $(g-2)_\mu/2$. *Physical Review D*, 80(11):114024, 2009.

[91] GJ Gounaris and JJ Sakurai. Finite-width corrections to the vector-meson-dominance prediction for $\rho \to e^+e^-$. *Physical Review Letters*, 21(4):244, 1968.

[92] Heath Bland O'Connell, BC Pearce, Anthony W Thomas, and Anthony G Williams. Rho-omega mixing and the pion electromagnetic form-factor. *Physics Letters B*, 354(1-2):14–19, 1995.

[93] Kim Maltman, Heath Bland O'Connell, and Anthony G Williams. Analysis of rho-omega interference in the pion form-factor. *Physics Letters B*, 376(1-3):19–24, 1996.

[94] Heath Bland O'Connell, BC Pearce, Anthony W Thomas, and Anthony G Williams. Constraints on the momentum dependence of rho-omega mixing. *Physics Letters B*, 336(1):1–5, 1994.

[95] Maarten Golterman, Kim Maltman, and Santiago Peris. New strategy for the lattice evaluation of the leading order hadronic contribution to $(g-2)_\mu$. *Physical Review D*, 90(7):074508, 2014.

[96] Maarten Golterman, Kim Maltman, and Santiago Peris. Tests of hadronic vacuum polarization fits for the muon anomalous magnetic moment. *Physical Review D*, 88(11):114508, 2013.

[97] Alexander Keshavarzi. The muon g- 2 experiment at Fermilab. In *EPJ Web of Conferences*, volume 212, page 05003. EDP Sciences, 2019.

[98] Jonathan Link. The standard model of physics is a tyrant. 2018.

[99] Julian Schwinger. On quantum-electrodynamics and the magnetic moment of the electron. *Physical Review*, 73(4):416, 1948.

[100] Michel Davier, Andreas Hoecker, Bogdan Malaescu, and Zhiqing Zhang. Reevaluation of the hadronic vacuum polarisation contributions to the standard model predictions of the muon $g-2$ and $\alpha(m_z^2)$ using newest hadronic cross-section data. *The European Physical Journal C*, 77(12):827, 2017.

[101] Harold W Fearing and Stefan Scherer. Extension of the chiral perturbation theory meson Lagrangian to order p^6. *Physical Review D*, 53(1):315, 1996.

Appendix

Relations between the Physical Pseudoscalar Fields and the Cartesian Components, ϕ_a

$$\pi^+ = \frac{1}{\sqrt{2}}(\phi_1 - i\phi_2), \tag{1}$$

$$\pi^- = \frac{1}{\sqrt{2}}(\phi_1 + i\phi_2), \tag{2}$$

$$K^+ = \frac{1}{\sqrt{2}}(\phi_4 - i\phi_5), \tag{3}$$

$$K^- = \frac{1}{\sqrt{2}}(\phi_4 + i\phi_5), \tag{4}$$

$$K^0 = \frac{1}{\sqrt{2}}(\phi_6 - i\phi_7), \tag{5}$$

$$\bar{K}^0 = \frac{1}{\sqrt{2}}(\phi_6 + i\phi_7), \tag{6}$$

In the isospin symmetric limit,

$$\pi^0 = \phi_3, \tag{7}$$

$$\eta = \phi_8. \tag{8}$$

Isospin breaking, $m_u \neq m_d$, establishes a mixing term in the mass-squared matrix. The physical particles correspond to eigenvectors of this matrix which, assuming $(m_d - m_u)$ to

be small so that we can keep only terms up to first order in it, can be written as

$$\pi^0 \simeq \phi_3 + \theta_0 \phi_8 \tag{9}$$

$$\eta \simeq \phi_8 - \theta_0 \phi_3 \tag{10}$$

where

$$\theta_0 = -\frac{m^2_{\phi_3\phi_8}}{m^2_{\phi_8} - m^2_{\phi_3}} = \frac{\sqrt{3}}{4}\frac{m_d - m_u}{m_s - \hat{m}} \tag{11}$$

where $\hat{m} = \frac{1}{2}(m_u + m_d)$.